



# VCU

Virginia Commonwealth University  
VCU Scholars Compass

---

Theses and Dissertations

Graduate School

---

2017

## NANOCOMPOSITE BIOELECTRONICS FOR BIOPOTENTIAL ENABLED PROSTHESIS

Dong Sup Lee  
*Virginia Commonwealth University*

Follow this and additional works at: <https://scholarscompass.vcu.edu/etd>



Part of the [Biomechanical Engineering Commons](#)

© The Author

---

Downloaded from

<https://scholarscompass.vcu.edu/etd/4836>

This Thesis is brought to you for free and open access by the Graduate School at VCU Scholars Compass. It has been accepted for inclusion in Theses and Dissertations by an authorized administrator of VCU Scholars Compass. For more information, please contact [libcompass@vcu.edu](mailto:libcompass@vcu.edu).

Dong Sup Lee, May 2017

All Rights Reserved.

**NANOCOMPOSITE BIOELECTRONICS FOR BIOPOTENTIAL ENABLED  
PROSTHESIS**

A thesis submitted in partial fulfillment of the requirements for the Degree of Master of Science  
at Virginia Commonwealth University.

By

Dong Sup Lee

Advisor: Dr. Woon-Hong Yeo

Assistant Professor

Department of Mechanical and Nuclear Engineering, School of Engineering,

Center for Rehabilitation Science and Engineering, Massey Cancer Center, School of Medicine,

Virginia Commonwealth University

Richmond, Virginia

May, 2017

## **Acknowledgements**

I would like to articulate sincere appreciation to Professor Woon-Hong Yeo for his professional guidance, valuable suggestions, constant encouragement and support to accomplish the study, and to Dr. Yongkuk Lee for sharing his knowledge and innovative ideas. In addition, hard work and help from fellow graduate student Saswat Mishra and undergraduate research assistants Andrew Choi, Youngbin Kim, Jookwang Lee are greatly appreciated.

## Table of Contents

Acknowledgements.....	ii
Table of Contents.....	iii
Table of figures.....	iv
Abstract.....	vii
Chapter 1: Introduction.....	1
Chapter 2: Introduction to biopotential.....	3
Chapter 3: Working Principle.....	6
3.1 Electrode to skin impedance of soft, stretchable electrode on skin.....	6
3.2 Conductivity and preparation of conductive polymer nanocomposite.....	9
Chapter 4: Experimental study.....	12
4.1 Mechanical and electrical properties test.....	12
4.2 Stretchability test and finite element analysis of conductive polymer electrode.....	20
Chapter 5: Application study.....	22
5.1 Electromyogram measurement.....	22
5.2 Electromyogram application to control prosthetic arm.....	24
Chapter 6: Conclusion.....	30
List of references.....	32
Appendices.....	36
Vita.....	60

## Table of figures

Figure 1. Cell membrane showing exchange of sodium and potassium ions. <sup>20</sup> .....	3
Figure 2. Schematic drawing showing flow of action potential in one direction. <sup>20</sup> .....	5
Figure 3. Half-and-Half fractal pattern derived from repeating units of ‘Peano’ curves. Fractal curves ensure high-density space filling. <sup>18</sup> .....	6
Figure 4. Electrical model of gel and dry electrodes. ....	8
Figure 5. Conductive polymer based electrode on skin. ....	9
Figure 6. Nanocomposite preparation method. ....	10
Figure 7. Composition of samples and image of uniaxial stretching test while measuring its resistance. ....	11
Figure 8. Uniaxial testing of samples #1-3. ....	13
Figure 9. Sheet resistance of samples #4-6 that have same composition of CB, CNT, AgNW, and PDMS but different mixing time with overhead mixer. ....	15
Figure 10. Stress and strain graph of sample #6. ....	16
Figure 11. Stress and strain curve of samples #6 and 7 that shows enhancement of mechanical properties by adding DS. ....	17
Figure 12. Fabrication of patterned mold and electrode on a thin elastomeric membrane. ....	19
Figure 13. Biaxial stretching of fabricated electrode. ....	20
Figure 14. Finite element analysis of our electrode design. ....	20
Figure 15. Signal flow diagram. ....	22
Figure 16. EMG signal measurement set-up on the flexor muscle to record squeezing signal of the arm. ....	23

Figure 17. EMG signal comparison of conventional gel electrode and embossed fractal electrode. .....	24
Figure 18. Parts of prosthetic arm retrieved from open source InMoove. Image of assembling each parts. Photo of rotational motors assigned for movement of each fingers. Photo of completed prosthetic arm. ....	25
Figure 19. Prosthetic arm control set-up with three EFE electrodes on different mounting sites on the forearm. ....	26
Figure 20. Different motions and corresponding signal from each channel. ....	27
Figure 21. Comparison of confusion matrix accuracy (7 classes) between the conventional gel electrode and embossed fractal electrode (EFE). ....	29

### List of Tables

Table 1. List of samples with different composition that are used for uniaxial stretching test. ...	12
Table 2. Average of resistance measured during uniaxial stretching test. ....	13
Table 3. List of samples with different mixing time that are used for sheet resistance measurement. ....	14
Table 4. Sheet resistance of samples #4-6. ....	15
Table 5. Samples compared with stress and strain measurement. ....	16
Table 6. Young's modulus of nanocomposites and pure PDMS calculated by getting the slope of elastic portion in figure 11. ....	18

### **Abstract**

Soft material-enabled electronics can demonstrate extreme mechanical flexibility and stretchability. Such compliant, comfortable electronics allow continuous, long-term measurement of biopotentials on the skin. Manufacturing of the stretchable electronic devices is enabled by the recent development combining materials transfer printing and microfabrication. However, the existing method using inorganic materials and multi-layered polymers requires long material preparation time and expensive processing cost due to the requirement of microfabrication tools and complicated transfer printing steps. Here, this study develops a new fabrication method of soft electronics via a micro-replica-molding technique, which allows fast production, multiple use, and low cost by avoiding microfabrication and multiple transfer printing. The core materials, carbon nanomaterials integrated with soft elastomers, further reduces the entire production cost, compared to costly metals such as gold and silver, while offering mechanical compliance. Collectively, skin-wearable electrodes, designed by optimized materials and fabrication method enable a high-fidelity measurement of non-invasive electromyograms on the skin for advanced human-machine interface, targeting prosthesis.

## Chapter 1: Introduction

Electro-physiological signals have been useful in various applications ranging from clinical diagnostics to human machine interfaces.<sup>1</sup> Especially electromyogram (EMG), which stands for three Greek words, ‘electron’ for use of electricity, ‘myos’ for ‘muscle’ and ‘graph’ for ‘writing’, is one of electro-physiological that records electrical signal from the muscle activity that used to investigate muscle conditions and diagnosis for neuromuscular disorders for further rehabilitations.<sup>2</sup> Another useful application of EMG is to control prosthetics to support people with physical disabilities.<sup>3</sup> To drive prostheses such as artificial limbs<sup>4</sup> and exoskeletons<sup>5</sup>, it requires electrode that acquires signal, data acquisition device that transmits signal to control interface, control interface that analyzes and classifies signal, and output device that receives control command from control interface.<sup>6</sup> In this thesis, general prosthetic arm is designed and built by using open source information from InMoov and the main focus of the thesis will be on developing an electrode that is needed to acquire EMG signal.

Acquiring high quality EMG signal is essential for accurate control of prosthesis. For EMG measurement, powerline noise and the cable motion artifact can be completely eliminated by filtering specific frequency ranges but skin movement caused by inadequate electrode to skin contact must be removed for better signal quality.<sup>7</sup> Thus for high quality EMG signal, skin-electrode interface must be carefully designed; material selection, geometry, and dimensions of the electrode.<sup>8</sup> A traditional method of recording EMG signal involves electrodes with electrolyte gel for efficient electrical coupling through reduced electrode to skin impedance.<sup>9</sup> However, there are potential problems of using gel electrodes, they cause skin irritation (erythema), user discomfort, and signal degradation due to gel drying out over few hours.<sup>10-12</sup> Therefore, electrodes

without incorporating electrolyte gel, so called dry electrodes are introduced to overcome issues of using gel based electrodes.<sup>13</sup> Dry electrodes are made by processing metal such as gold through microfabrication techniques involving photolithography thus dry metal based electrodes often require multi-complex preparation steps, expensive machines, expensive materials, and inconvenient mechanical fixtures.<sup>14</sup> In order to reduce the cost and complicated microlithography fabrication steps, carbon-polymer based dry electrode through molding technique is introduced.<sup>15</sup> The key to make polymer based electrode is to achieve its conductivity of at least  $1S/m$  for successful electrical signal measurement.<sup>16</sup> In order to maximize conductivity, different conductive materials such as carbon nanotube (CNT)<sup>17</sup>, carbon black (CB)<sup>18</sup>, and silver nanowire (AgNW)<sup>19</sup> composite electrodes have been introduced. The major advantages of using conductive polymer based electrodes is that they do not require any additional adhesive or electrolytic gel so they can be immediately and conveniently used. Also, the conductive materials added to the polymer are relatively cheap compare to materials added to make metallic electrodes. However, due to high resistivity of the polymer, they get easily disturbed by motion artifacts.<sup>20</sup> Also, previously introduced conductive polymer based electrodes are made in a sheet in which application sites on the skin will be limited because skin can stretch up to 20% and 50% for joints.<sup>21</sup> The conductive polymer sheet is not capable of stretching up to 50%. In addition to limited stretchability, they have insufficient adhesion to the skin because they lose adhesion when mixed with conductive materials. Thus, in this thesis I propose embossed fractal electrode (EFE) made of conductive polymer, which can potentially be used on any part of the body due to high stretchability and it has sufficient adhesion on the skin without any adhesives.

## Chapter 2: Introduction to biopotential

Generation of biopotential signal, measurement of electrical activity in biological nerves and tissues, is due to electric potential difference at the cell membrane that results from difference in ionic concentration at outside and inside the cell.<sup>22</sup> The cell membrane has many active sodium-potassium-ATPase pumps, which pumps three sodium ions outside the membrane for an exchange of two potassium ions shown in figure 1.

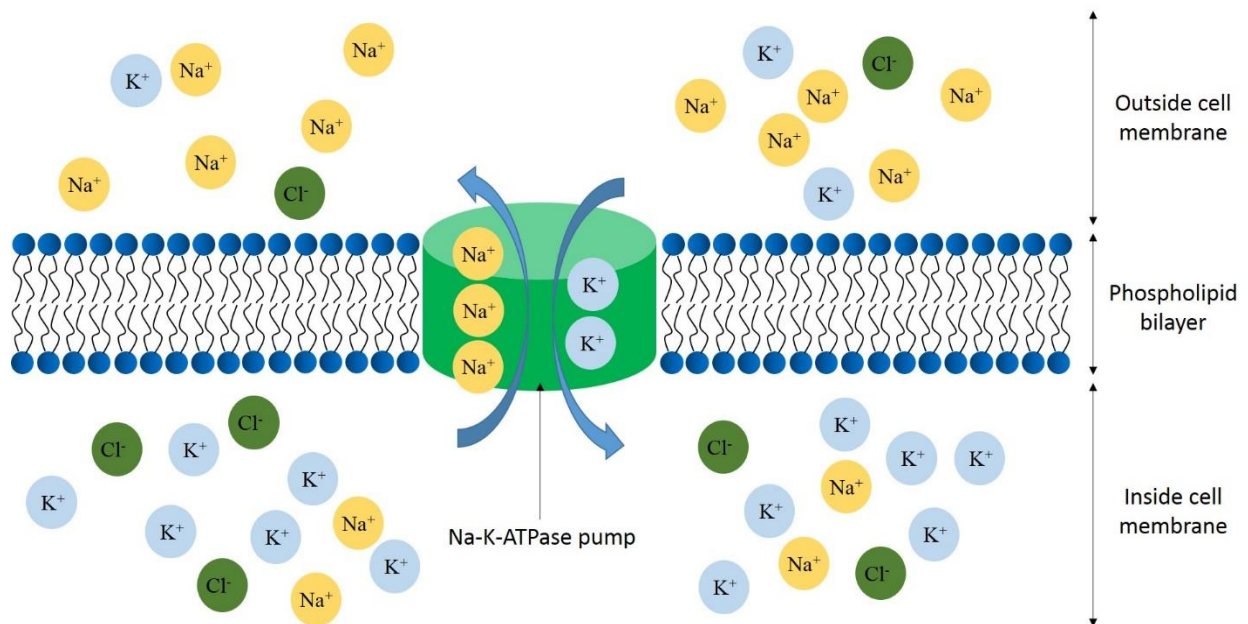


**Figure 1.** Cell membrane showing exchange of sodium and potassium ions.<sup>23</sup>

When cell membranes is at rest, the membrane is more permeable to potassium and chlorine ions and there is high concentration of potassium ions inside the cell and high concentration of sodium ions outside the cell.<sup>24</sup> The potential difference at rest, known as resting potential, can be calculated by Nernst equation:

$$V = \frac{RT}{zF} \ln \frac{[\text{ion concentration outside cell}]}{[\text{ion concentration inside cell}]}$$

where,  $V$  is voltage,  $R$  is gas constant,  $T$  is temperature,  $z$  is valence of the ionic species, and  $F$  is Faraday's constant.<sup>25</sup>

Due to high concentration of potassium ions inside cell and, high concentration of sodium outside the cell, the equilibrium potential of potassium and chlorine ions are negative and the equilibrium potential of sodium is positive.<sup>26</sup> Thus, there is net positive charge outside membrane and net negative charge inside the membrane and the difference in charge between outside and the inside the neuron cell called resting potential is approximately  $-70\text{mV}$ .<sup>27</sup> When the cell excites, so called action potential occurs, electric gradient of the cell changes due to opening of sodium channels, which results in rapid flow of sodium ions inside the cell.<sup>28</sup> The rapid movement of sodium ions, also known as depolarization, causes electrical potential to change from  $-70\text{mV}$  to above  $+35\text{mV}$  and it reverses the net charge inside and outside the cell so now inside the cell membrane becomes negative and outside the membrane becomes positive.<sup>25</sup> Once the spike in potential is introduced, it cannot react to additional stimuli the time it cannot receive additional stimuli is known as refractory period for about 1 milliseconds of refractory period,<sup>29</sup> the potassium channel opens completely and potassium ions diffuse out of the cell membrane leaving inside the membrane to be negatively charged again.<sup>25</sup> As potassium ions move out of the membrane known as repolarization, potential goes below the resting potential and the sodium-potassium-ATPase pump reestablishes the resting potential.<sup>30</sup> The sequence of depolarization and repolarization generates small electrical current in the localized area and the current at the localized area opens nearby sodium channels introducing action potential to nearby neurons.<sup>31</sup> Thus, the impulse passes down

the entire neuron in a direction from the dendrites toward the axon.<sup>20</sup> Figure 2 shows action potential flow in a neurological level.

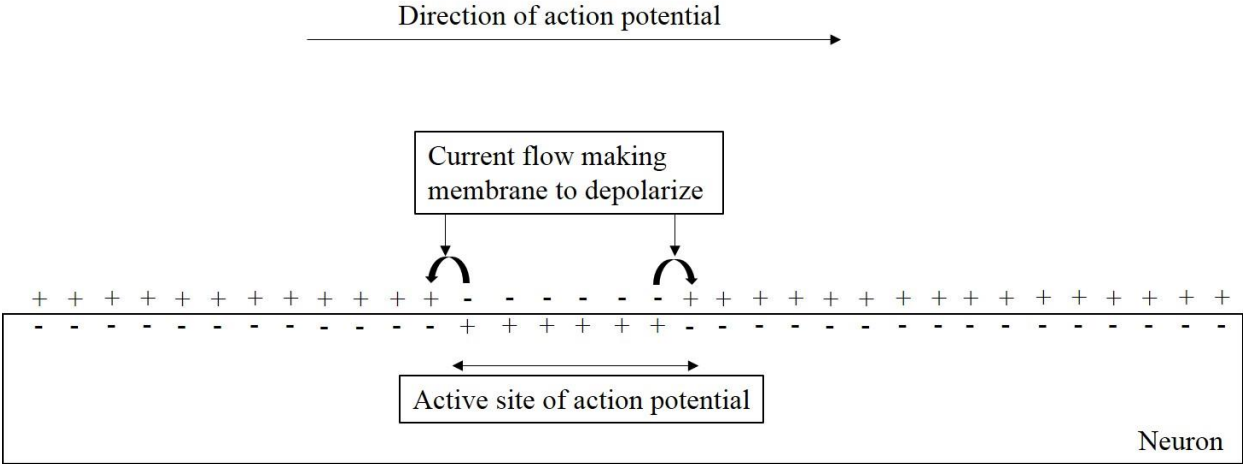
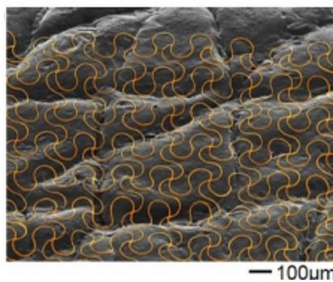


**Figure 2.** Schematic drawing showing flow of action potential in one direction.<sup>23</sup>

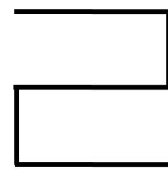
## Chapter 3: Working Principle

### 3.1 Electrode to skin impedance of soft, stretchable electrode on skin.

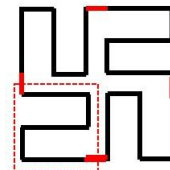
Recent studies show that stretchability of the skin-like electrodes must exceed stretchability of the skin (10-20%) to ensure mechanical stability when applied on the skin.<sup>21</sup> The result of stretching different space-filling curves like ‘von Koch’, ‘Peano’, ‘Hibert’, ‘Moore’, ‘Vicsek’, ‘Greekcross’ show that ‘Peano’ curve can stretch the most when same maximum principal strain is introduced, in addition, the study shows that Half-and-half fractal pattern, representing repeating units of ‘Peano’ curve, has good balance of stretchability at both x-axis and y-axis when stretched biaxially.<sup>32</sup> The stretchability of rigid metal such as gold could be stretched more than 50% if fabricated in thin Half-and-half fractal pattern.<sup>21</sup> Figure 3 presents Half-and-half fractal curve derived from single ‘Peano’ curve with arc corners to reduce elastic stress concentration at the sharp corners. Rigid gold material is fabricated in a thin open-mesh pattern so it becomes flexible and stretchable. The flexible and stretchable properties ensures the metal electrode to have conformal contact with skin and sustain its functionality even when the skin stretches. Thus, Half-and-half fractal pattern is implemented when designing an electrode.



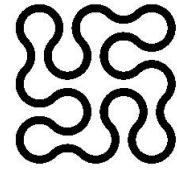
Gold based electrophysiological signal sensor with stretchable geometry on skin



‘Peano’ curve



Half-and-half fractal formed by repeating units of ‘Peano’ curve



Half-and-half fractal with arc at the corner

**Figure 3.** Half-and-Half fractal pattern derived from repeating units of ‘Peano’ curves. Fractal curves ensure high-density space filling.<sup>21</sup>

When using dry electrode instead of gel electrode, it is important to make sure that the dry electrodes are as equally operational as gel electrodes because dry electrodes lack conductive gel, which assists in both electrodes to skin impedance and potential measured between electrode and the surface of the skin. Figure 4 represents equivalent electrode-skin interface model for both gel and dry electrodes. The generated potential is denoted by  $E_{hc}$ , the electrode-skin interface is modeled by a double layer structure by capacitor  $C_d$  and a resistor  $R_d$  with parallel connection,  $R_s$  denotes resistance of electrolytic gel with high concentration of ions,  $E_{se}$  expresses ionic concentration difference across the epidermis,  $C_e$  and  $R_e$  refer to epidermis exhibiting both capacitive and resistive behavior, and  $R_u$  represents dermis that can be treated as pure resistor.<sup>33</sup> Although dry electrodes omit electrolytic gel between the electrode and the surface of the skin, perspiration of the skin after several minutes of mounting would moisturize the skin under the dry electrode and it can overcome the absence of electrolyte gel.<sup>13</sup> Since the study claims that the absence of conductive gel would have no effect on biopotential measurement if low electrode to skin impedance is achieved; since dry electrodes do not have conductive gel that helps reducing electrode to skin impedance, it is important to design dry electrode in a way that it would have low electrode to skin impedance even without conductive gel, otherwise, dry electrode would have high baseline noise upon measuring EMG signal.

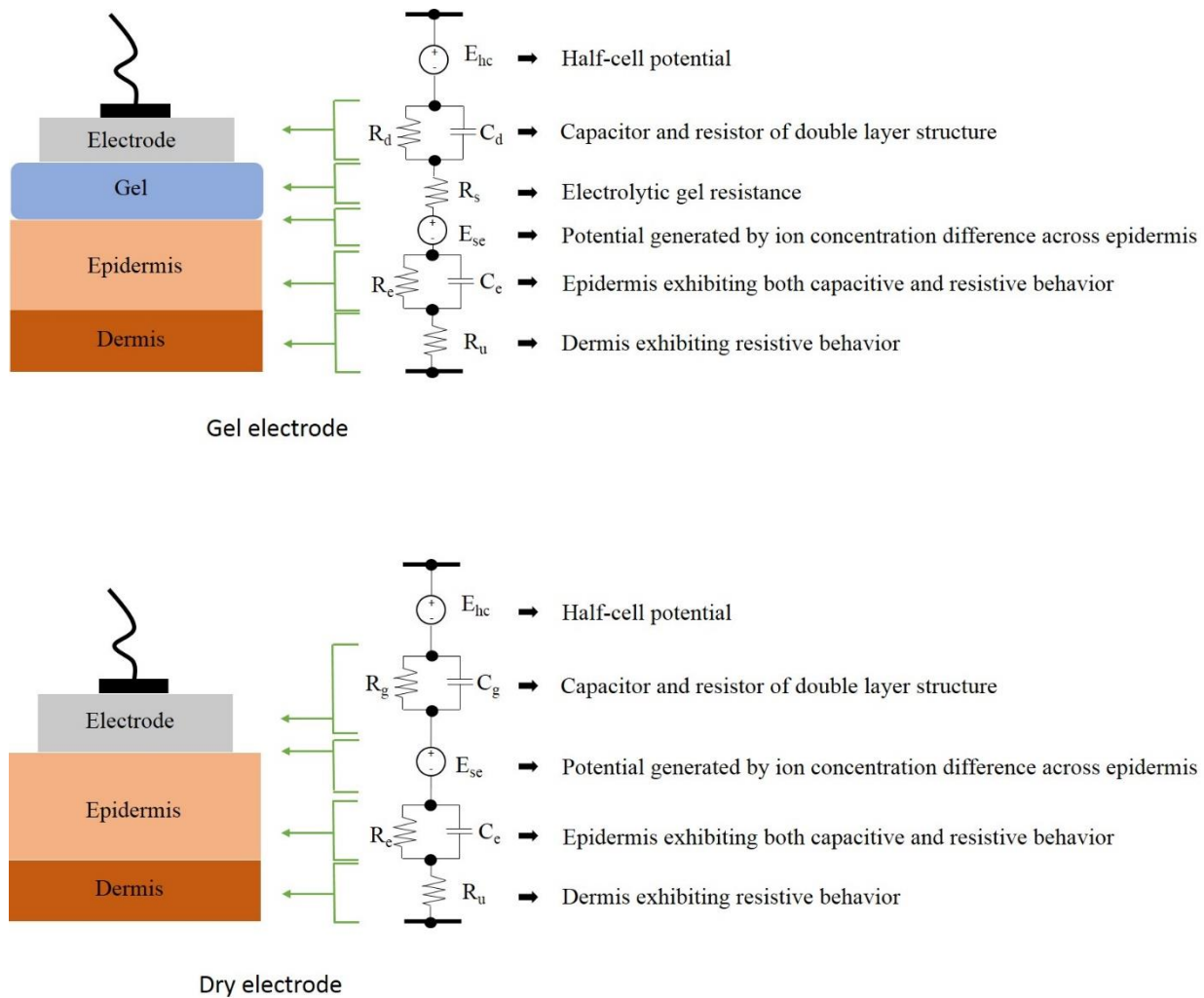


**Figure 4.** Electrical model of gel and dry electrodes.

As I mentioned previously, electrode to skin impedance is one of the crucial factor that affects the quality of electrophysiological signal. To achieve low electrode to skin impedance, electrode must have conformal contact with the skin because reducing the gap between the electrode and skin will decrease the impedance between the electrode and the skin. In order to achieve conformal contact with curvilinear shape of the skin, electrodes need to be flexible and the thickness of elastomeric membrane that hold electrode needs to around  $5\mu\text{m}$  to minimize the gap between the electrode and the skin.<sup>34</sup> The embossed fractal electrode (EFE) is made of

conductive polymer and fabricated on a thin elastomeric membrane substrate to ensure conformal contact on the skin. The flexible and stretchable properties of polymer enables EFE to stretch beyond the stretchability of the skin to assure its functionality without fracture even on stretched skin surface. Also, the adhesion of the elastomeric membrane provides sufficient adhesive force between the electrode and the skin but not excessive to cause skin irritation upon removal. The absence of conductive gel will prevent any potential allergic reaction. Figure 5 presents estimated modeling of EFE on the curvilinear morphology of the skin.

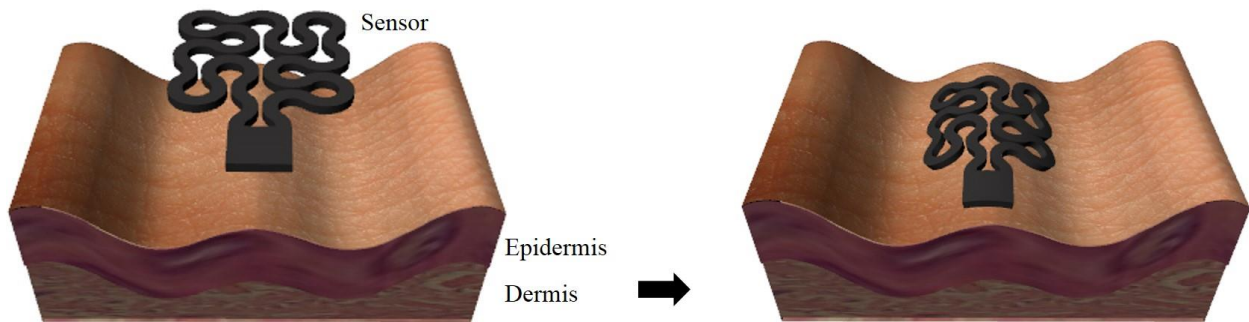


**Figure 5.** Conductive polymer based electrode on skin.

### 3.2 Conductivity and preparation of conductive polymer nanocomposite.

Preparation of conductive polymer is one of the critical step to generate EFE because it is directly related to the conductivity of the electrode. Finding appropriate conductive materials and weight percentage of each conductive material is important because the conductivity of nanocomposite material depends on how much conductive materials are mixed with the polymer. Carbon nanotube (CNT) is used as a major material for making conductive polymer because it has high conductivity, low sensitivity to surrounding magnetic field, and the price is relatively low when compared to metal nano-particles like gold. In addition to CNT mixture, carbon black (CB) is added because pure CNT-polymer mixture would have small gaps between CNTs so by adding

CB, the gaps are minimized. In order to maximize the conductivity of the carbon-based nanocomposite, silver nanowires (AgNW) are also added because silver is known for extremely high conductivity, however, price of AgNW is relatively high when compared to carbon materials, thus very small amount of AgNW are added to the mixture. In addition to finding composition of the nanocomposite, it is important to make sure the composite materials are mixed thoroughly. The conductive materials must be uniformly mixed and spread through the polymer medium so there is uniform electrical connectivity throughout the mixture. To find appropriate weight percentage of each conductive materials and mixing time, nanocomposites containing conductive materials with different weight percentages are prepared by following method in figure 6. First, CB, CNT, and AgNW are mixed with polydimethyl-siloxane (PDMS) base using the mechanical stirrer. Then, PDMS curing reagent is added to the mixture in 10:1 base to curing reagent ratio.

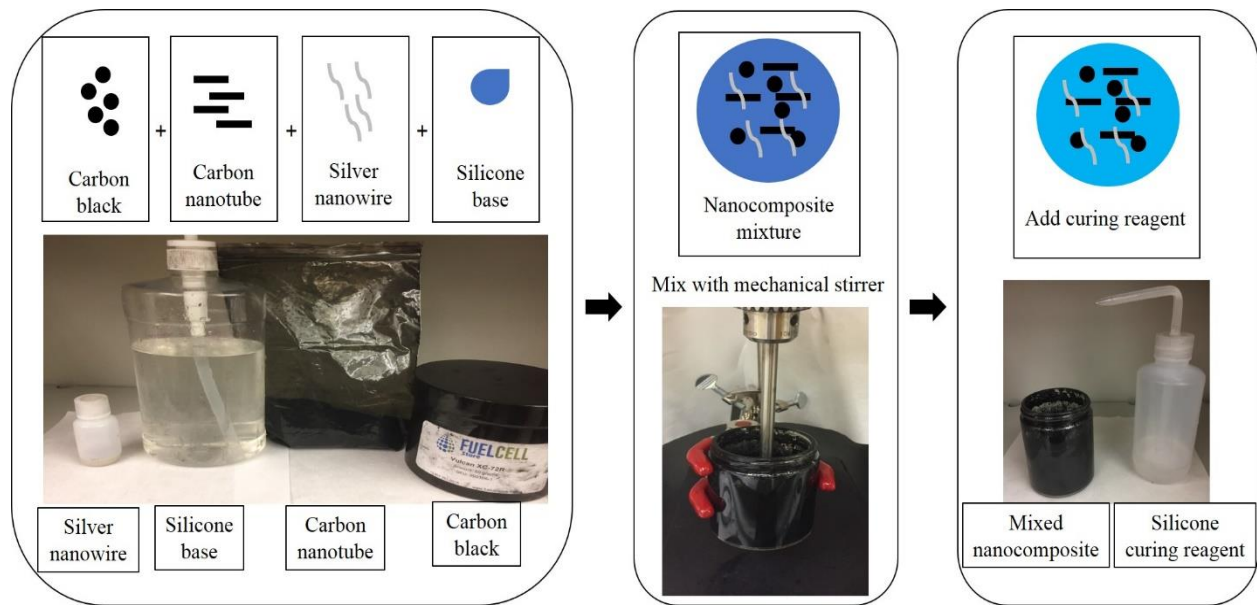


**Figure 6.** Nanocomposite preparation method.

There are two major factors contributing to the quality of the signal. Previously, I mentioned about the electrode to skin impedance that contributes to the noise level of the signal,

and the conductivity of the electrode, which is related to the amplitude of the signal. Higher signal amplitude can be achieved through higher conductivity. Since EFE is made of conductive polymer, it is important to maximize the conductivity of the conductive polymer mixture. Higher conductivity is achieved by adding higher weight percentage of carbon and silver materials but there is a limitation of how much it can be added to the polymer. If conductive materials are added over its limitation, the mixture becomes too viscous that it would not mix well then it cannot be used as a replica material to generate EFE because it would not fill the gaps of the mold. To find suitable composition for EFE, samples with different composition are made to examine its properties. Also, samples with different mixing time are prepared to find out the reasonable mixing time of the conductive materials and the polymer. Lastly, DragonSkin (DS) is added to the mixture to enhance the mechanical strength of the nanocomposite. Figure 7 presents size of the sample prepared for testing and uniaxial stretching test set-up.

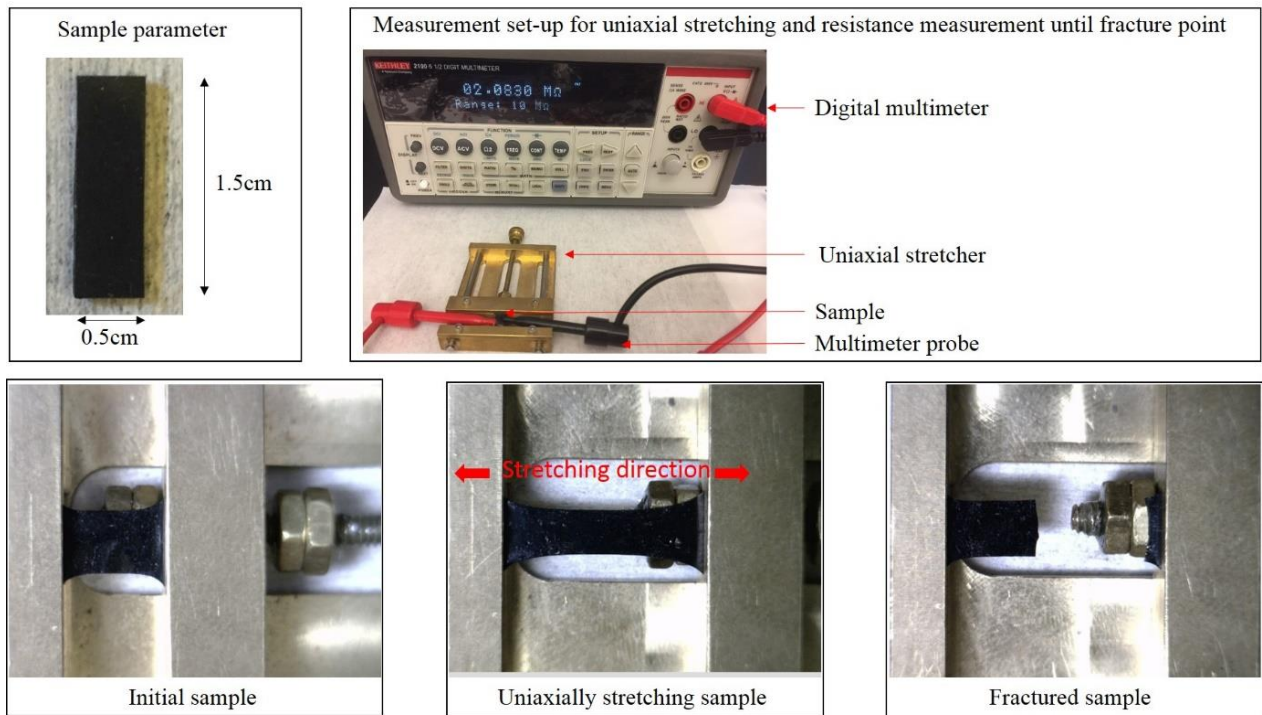


**Figure 7.** Experimental study of the mechanical stretchability of a fabricated electrode.

## Chapter 4: Experimental study

### 4.1 Mechanical and electrical properties test

Table 1 shows the list of samples with different composition in which resistance is measured while stretching uniaxially. The resistance measurement while stretching the sample would provide information of how different composition affects its conductivity and mechanical strength while stretched.

Sample number	Sample type
#1	10% Carbon black (CB) + 5% Carbon nanotube (CNT) + 85% Polydimethyl siloxane (PDMS) mixed for 2 hours
#2	10% CB + 2.5% CNT + 0.4% Silver nanowire (AgNW) + 87.1% PDMS mixed for 2 hours
#3	10% CB + 5% CNT + 0.4% AgNW + 84.6% PDMS mixed for 2 hours

**Table 1.** List of samples with different composition that are used for uniaxial stretching test.

Figure 8 demonstrates the result of uniaxial stretching test in which followed what was predicted; more conductive materials added to the composite, lower resistance it would be. Table 2 shows average resistance values measured during uniaxial stretching test. It shows that sample #3 has lowest resistance measured, followed by sample #1 and #2. From the data, resistance of the nanocomposite depends a lot on the amount of CNT because sample #3 recorded lower resistance compare to that of sample #2 and the resistance difference is over two order of magnitude for 2.5 weight percent difference in the amount of CNT. Also, the presence of 0.4 weight percent of AgNW affects resistance by an order of magnitude since resistance of sample #3 is more than an order of magnitude lower than that of sample #1 and the only difference is that sample #1 lacks AgNW. From the graph in figure 8, the fracture points of samples differ; the stretchability of the material is better if more polymer is added to the nanocomposite. To summarize, higher

conductivity is achieved through adding more conductive materials but there is a drawback of losing its stretchability; however, the stretchability of nanocomposite far exceed the stretchability of the skin (~20%), thus stretchability of nanocomposite can be neglected for our general purposes device application.

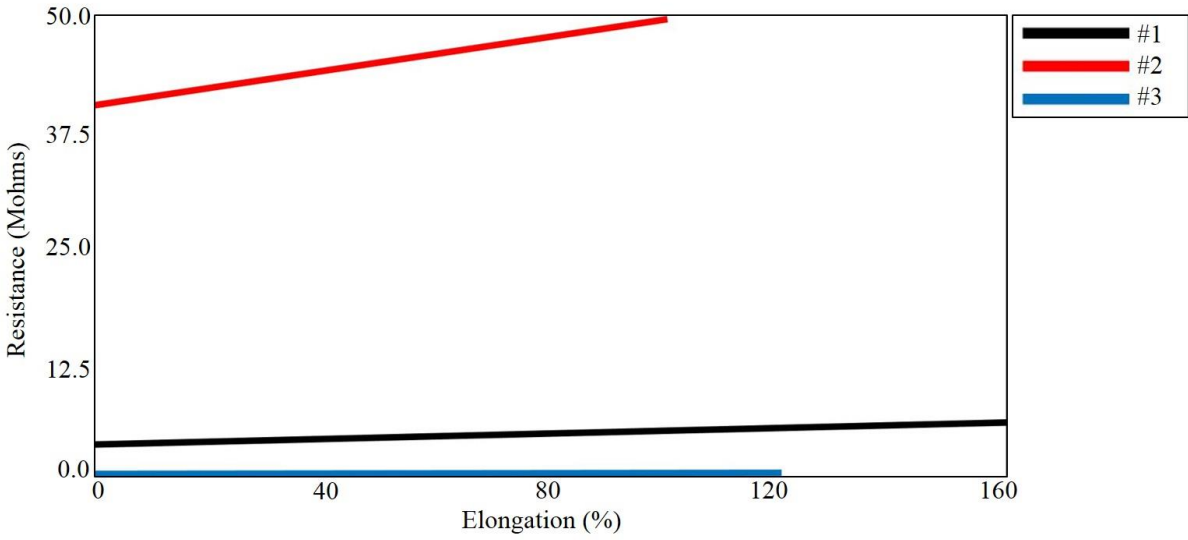


**Figure 8.** Uniaxial testing of samples #1-3.

Sample #	#1	#2	#3
Resistance average (Mohms)	4.63	51.2	0.39

**Table 2.** Average of resistance measured during uniaxial stretching test.

Finding the appropriate mixing time of the conductive materials and the polymer is one of the crucial factors that define conductivity of the nanocomposite. Conductive materials and polymer need to be uniformly mixed to achieve equal electrical connectivity throughout the mixture. In order to find appropriate mixing time to make nanocomposite, samples with different mixing time are prepared in table 3.

Sample number	Sample type
#4	10% CB + 5% CNT + 0.4% AgNW + 84.6% PDMS mixed for 5 hours
#5	10% CB + 5% CNT + 0.4% AgNW + 84.6% PDMS mixed for 10 hours
#6	10% CB + 5% CNT + 0.4% AgNW + 84.6% PDMS mixed for 15 hours
#7	10% CB + 5% CNT + 0.4% AgNW + 84.6% PDMS mixed for 20 hours

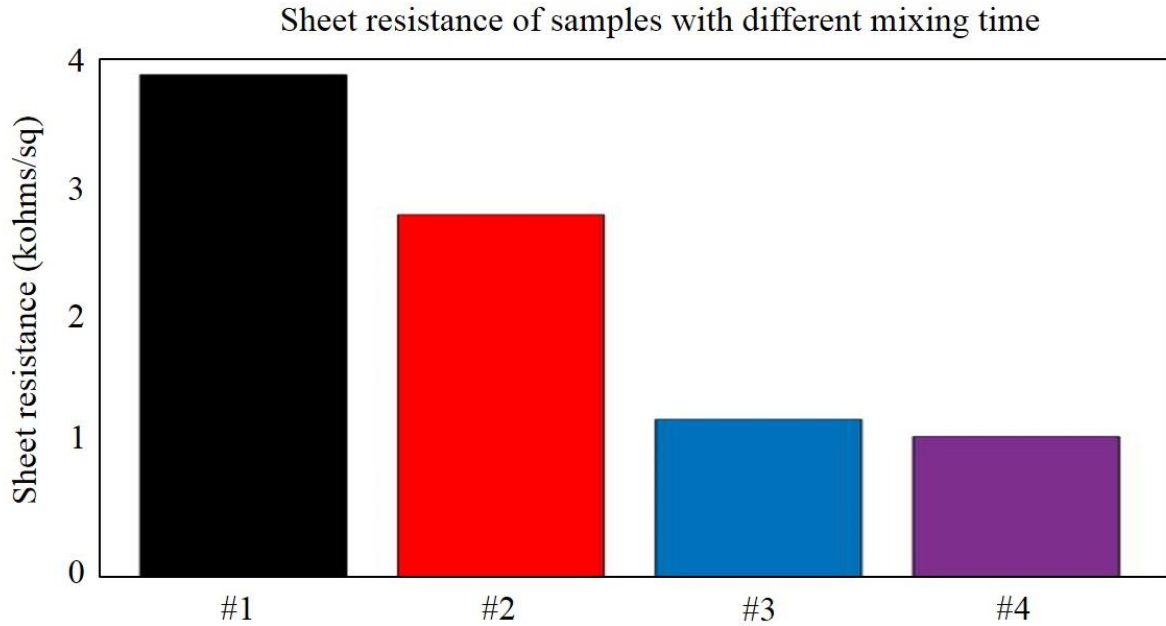
**Table 3.** List of samples with different mixing time that are used for sheet resistance measurement.

Figure 9 shows the sheet resistance measured with four point probe of samples #4, 5, 6, and 7 that have different mixing time of 5, 10, 15, and 20hours, respectively. The equation of sheet resistance measurement using four point probe is:

$$\text{Sheet resistance} = \frac{\pi}{\ln 2} \times \frac{V}{I} = 4.53 \frac{V}{I}$$

where  $I$  is current flow on outer probes and  $V$  is the voltage measured in inner probes.

From table 4, data shows that sample #6 has lowest sheet resistance than sample #4 and 5. The sheet resistance of sample #4 is more than three times than that of sample #6 and the sheet resistance of sample #5 is more than two times than that of sample #6. Beyond mixing time of 15hours, the sheet resistance stabilizes around 1.1kΩ/sq. Thus, longer the time of mixing with mechanical stirrer, better uniformity of sample can achieved and it is necessary to mix at least 15hours. Therefore, nanocomposite mixtures are prepared by mixing at least 15hours.



**Figure 9.** Sheet resistance of samples #4-6 that have same composition of CB, CNT, AgNW, and PDMS but different mixing time with overhead mixer.

Sample #	#4	#5	#6	#7
Average sheet resistance (kOhms / sq)	3.84	2.78	1.23	1.1

**Table 4.** Sheet resistance of samples #4-6.

Although the electrical properties of the mixture previously defined is suitable for the purpose of using it as an electrode on the skin, electrode pattern often gets disconnected while detaching replica from the mold. Also, figure 10 with stress and strain graph of sample #6 shows that material is does not have sufficient stretchability; its strain is less than 50% in which it is not appropriate for the use on joints.

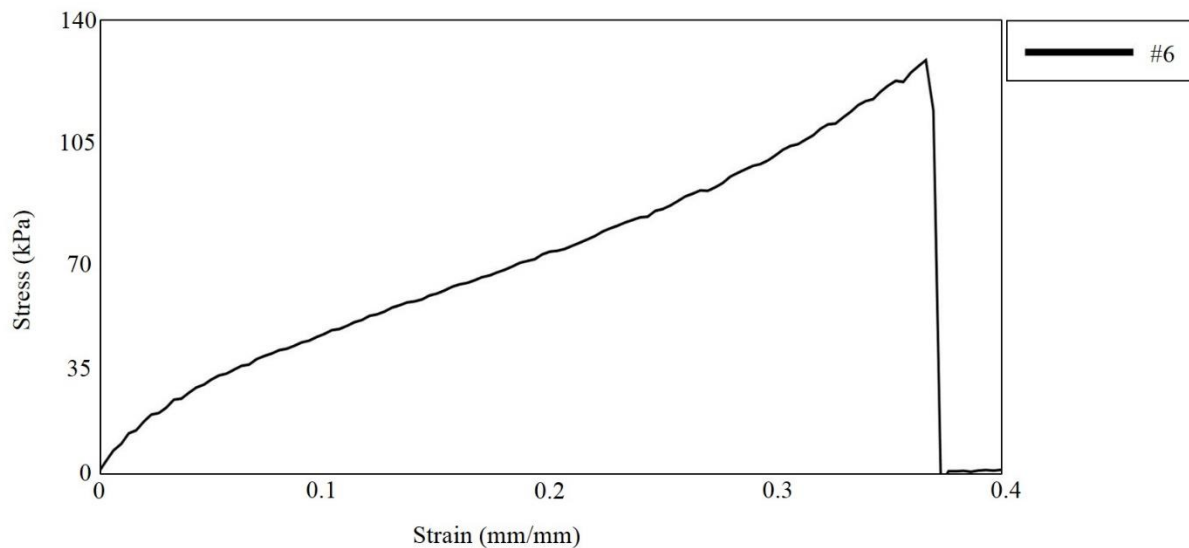


**Figure 10.** Stress and strain graph of sample #6.

Therefore, mechanics of material needs to be enhanced. I developed a novel way to enhance the material by adding another polymer called DragonSkin (DS). By replacing half of original PDMS weight with DS, the mechanical properties of the material enhanced more than twice of its original value and it is nearly three times the pure PDMS. Table 5 shows assigned samples tested for measuring stress and strain curve with Instron and figure 11 presents the result of the measurement.

Sample number	Sample type
#6	10% CB + 5% CNT + 0.4% AgNW + 84.6% PDMS mixed for 15 hours
#8	10% CB + 5% CNT + 0.4% AgNW + 42.3% PDMS + 42.3% DS mixed for 15 hours

**Table 5.** Samples compared with stress and strain measurement.

Young's modulus in table 6 shows measure of stiffness given by:

$$E = \frac{F/A}{\Delta L/L_0} = \frac{\sigma(\epsilon)}{\epsilon}$$

where, E is the Young's modulus, F is the force exerted on an object under tension, A is the actual cross-sectional area through which the force is applied,  $\Delta L$  is the amount by which the length of the object changes,  $L_0$  is the original length of the object,  $\sigma(\epsilon)$  is the tensile stress, and  $\epsilon$  is the extensional strain.

Our new material is approximately three times more stretchable without fracture than pure PDMS and PDMS nanocomposite. In other words, low Young's modulus of nanocomposite with DS is less resistance to deformation.

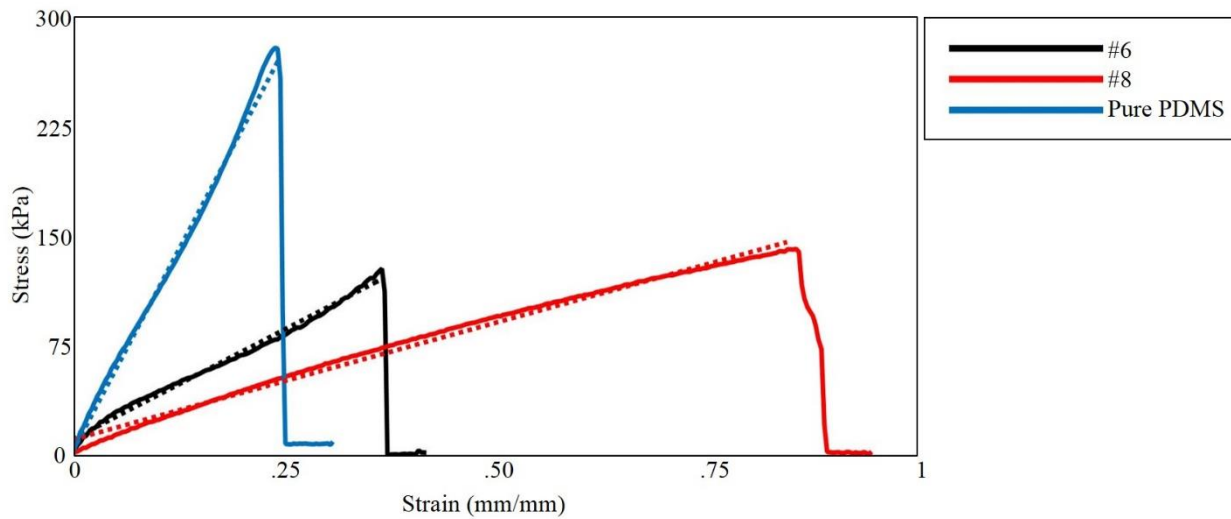


**Figure 11.** Stress and strain curve of samples #6 and 7 that shows enhancement of mechanical properties by adding DS.

Sample	Pure PDMS	#6	#8
Young's modulus (kPa)	1100	300	150

**Table 6.** Young's modulus of nanocomposites and pure PDMS calculated by getting the slope of elastic portion in figure 11.

The preparation of nanocomposite and testing its capability to use it as an electrode material is complete. Based on previous tests I optimized nanocomposite conductivity by reducing the amount of CB and maximizing the amount of CNT, thus new composition is 7 weight percent CB, 14 weight percent CNT, 0.5 weight percent AgNW, 39.25 weight percent PDMS, and 39.25 weight percent DS. The sheet resistance of new composite is 355  $\Omega/\text{sq}$ . Also, resistivity is measured to calculate its conductivity. The equation of resistivity measured through four point probe is given by:

$$\text{Resistivity} = \frac{V}{I} \times 2\pi \times s \times \frac{1}{G7}$$

where,  $I$  is the current flow on outer probes,  $V$  is the voltage measured in inner probes,  $s$  is the distance between probes (1270  $\mu\text{m}$ ),  $G7$  is a function of  $\frac{w}{s}$ ,<sup>35</sup> where  $w$  is the thickness of the substrate.

Measured resistivity of new sample is 44  $\Omega\text{-cm}$ , which is equivalent to 2.27  $S/m$  where it is above the recommended conductivity value for biopotential electrode ( $>1 S/m$ ). The conductivity is an inverse of resistivity:

$$\text{Conductivity} = \frac{1}{\text{Resistivity}}$$

Fabrication of mold with half-and-half fractal pattern involves basic photolithography techniques using photoresist, SU-8. The thickness of electrode can be adjusted by manipulating the thickness of the SU-8. I targeted our electrode height to be 250 $\mu$ m because less than 200 $\mu$ m depth mold is not capable of filling replica in the patterned mold by manually scraping the nanocomposite on the surface of the mold. The desired height is achieved by spin-coating two layers of SU-8 at 1300 rpm for 30 seconds, followed by pre-exposure bake, ultra violet exposure through a pattern, post-exposure bake, developing of SU-8, and hard bake. Once the mold is ready, the surface is silanized to prevent attaching of conductive nanocomposite on the mold, then scrape it with PDMS block to fill in the gaps. After curing nanocomposite, thin elastomer membrane is spin-coated on top to detach patterned nanocomposite from the mold. The thin elastomeric membrane ensures low electrode to skin contact impedance. Figure 12 shows general step by step method of fabricating patterned mold and electrode through replica molding process. Details of fabrication steps are discussed in Appendices I-II.

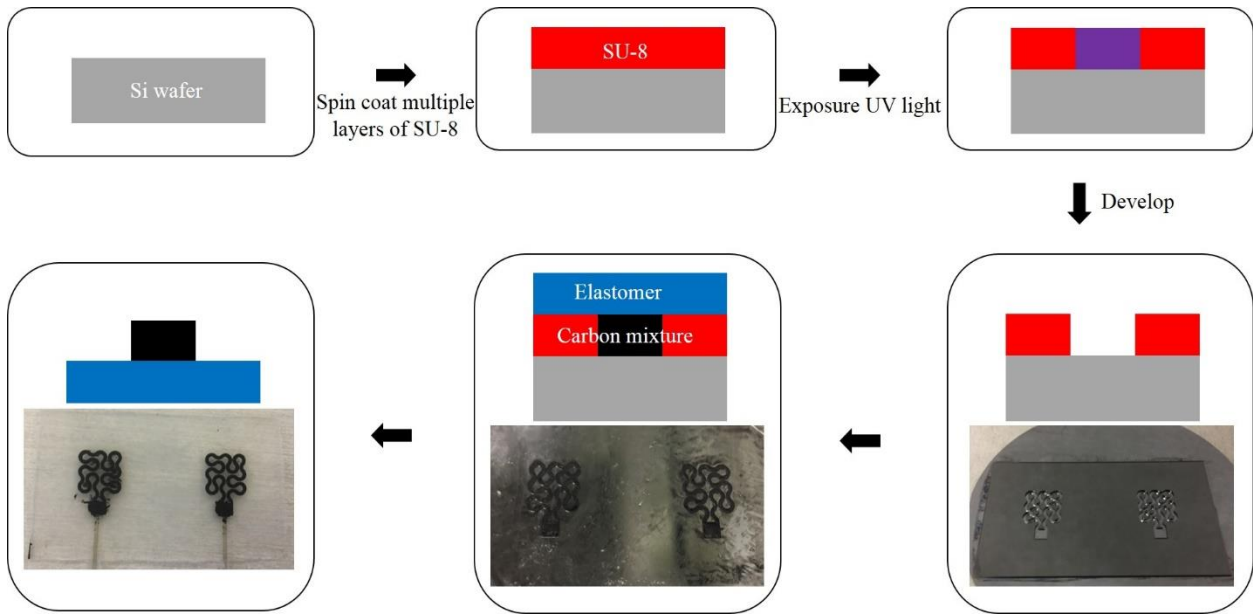


**Figure 12.** Fabrication of patterned mold and electrode on a thin elastomeric membrane.

## 4.2 Stretchability test and finite element analysis of conductive polymer electrode.

Biaxial testing allows visualization of stretched EFE pattern to ensure its capability of stretching without any mechanical failure. On average, our pattern started to show fracture at 200% of elongation. For the purpose our application, EFE meets the standard of operating on the skin without any failure, however, for the purpose of testing accuracy of finite element analysis data I compared biaxial testing in figure 13 with the result of finite element analysis in figure 14 to locate where maximum strain is held.

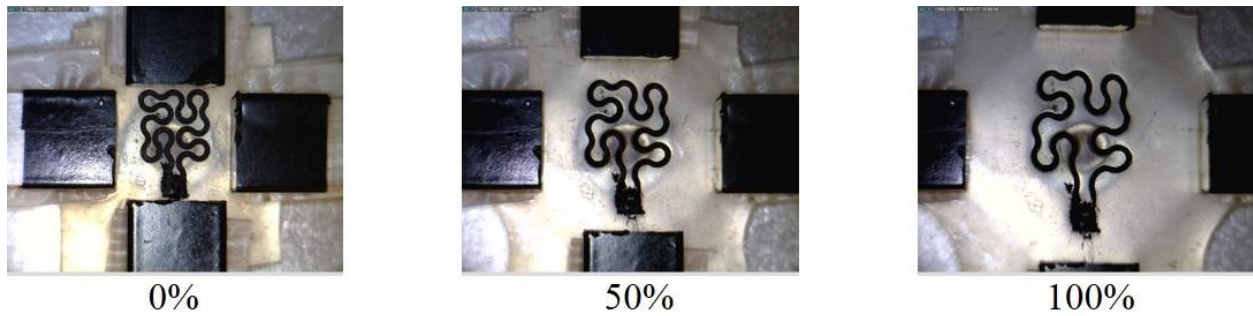


**Figure 13.** Biaxial stretching of fabricated electrode.

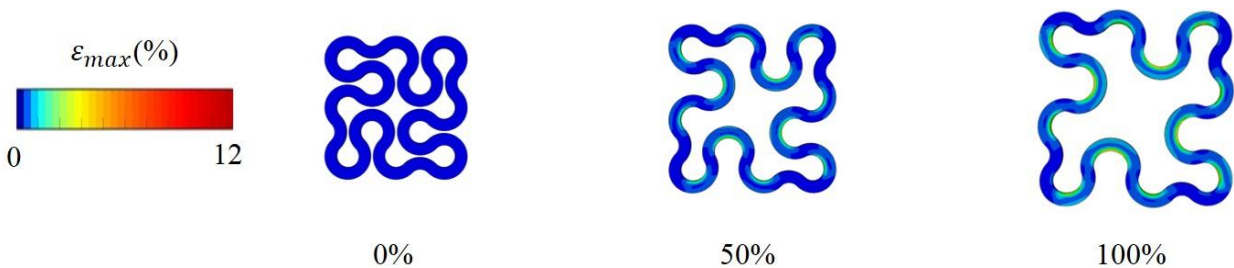


**Figure 14.** Finite element analysis of our electrode design.

For finite element analysis, Young's modulus, poisson's ratio, and density of EFE are considered. The Young's modulus of EFE with thin elastomeric membrane, which is 0.0005 MPa is taken into account. The density of EFE is estimated to be the average of PDMS density and DS density, which is  $1.0175g/cm^3$ . And the poisson's ratio is considered to be typical polymers,

which is 0.49. The result of actual biaxial stretching in figure 13 and predicted biaxial stretching in figure 14 are similar thus inputs for finite element analysis can be implemented when improving the design of the electrode. Finite element analysis shows that the highest stress assemble in the inner arc of the “Peano” curve. It is useful in a way that better electrode design can be generated and tested without actually fabricating electrodes.

## Chapter 5: Application study

### 5.1 Electromyogram measurement

Fabricated EFE can be used in different location of the human body to gather different types of electrophysiological signals. For our purpose of controlling prosthetic arm, electromyogram (EMG) is measured near flexor muscles on the forearm. Figure 15 presents signal flow diagram of the measured signal that will be processed to control the prosthetic arm. The signal measured through EFE will be transmitted using data acquisition device to a computer for feature extraction and classification that will control different motions of prosthetic arm.

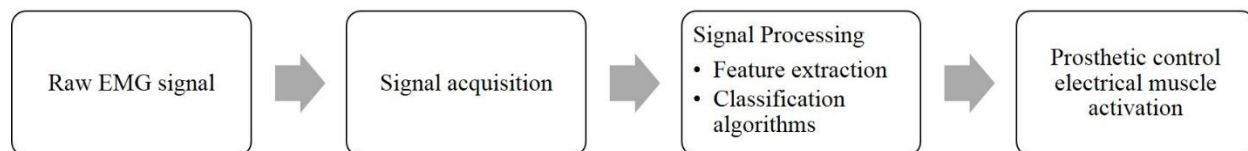


**Figure 15.** Signal flow diagram.

Before controlling the prosthetic arm, it is importance to investigate performance of EFE. The performance of electrode can be tested by comparing EMG signal measured using conventional gel electrode with that of EFE. Figure 16 demonstrates EMG signal measurement set-up using the EFE. Two electrodes are placed on the flexor muscle as measuring electrodes and ground electrode is placed on the tip of the ulna. EMG signal is measured while squeezing the flexor muscle. The hand dynamometer keeps track of the flexing force of the arm so each squeezing motions would have similar signal amplitude peaks. Details of finding signal to noise ratio of the collected data is discussed in Appendix III.

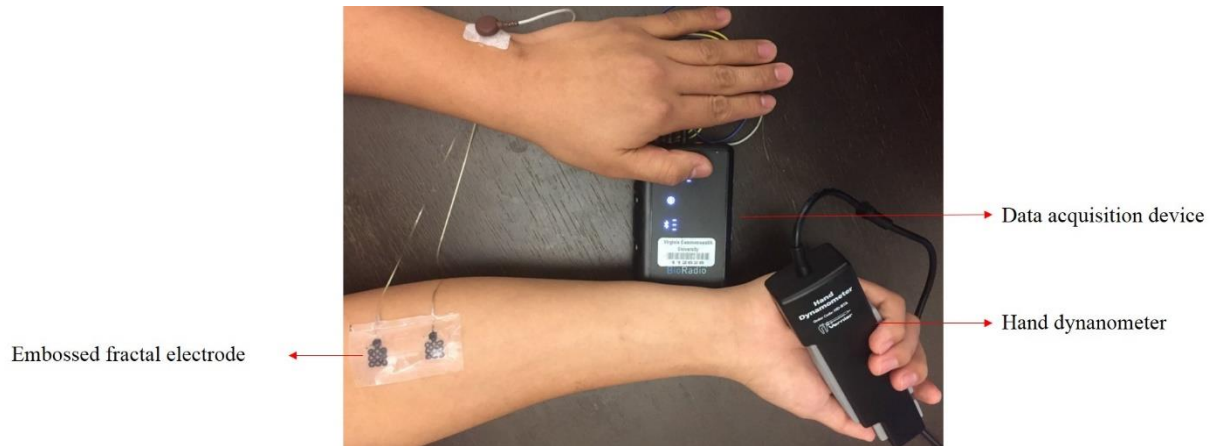


**Figure 16.** Photo of a EMG signal measurement set-up on the flexor muscle to record squeezing signal of the arm.

Comparison of EMG signal measured with conventional gel electrode and EFE is shown in figure 17. Continuous measurement of recording while subject squeezed arm every five seconds for ten times with 100N of squeeze force. The measurement was taken for three trials. The signal is filtered from 30Hz to 150Hz using the bandpass filter with a notch filter at 60Hz. The filtered signal is converted to root mean square graph to find amplitude peaks and noise to calculate signal to noise ratio (SNR). The baseline noise is defined to be the signal while in rest motion and signal amplitude is appointed to the signal peak during squeeze motion. Average noise level of electrodes are 0.00893mV and 0.01mV for conventional gel electrode and EFE, respectively. The average signal amplitude of conventional gel electrode is 0.318mV, and 0.3mV for the EFE. The difference in noise level is approximately 0.001mV, and the difference in signal amplitude is approximately 0.01mV. Thus, conventional gel electrode is better in both electrode to skin impedance and conductivity but difference is very small considering SNR of both electrodes. The SNR of  $31.06 \pm 0.85$  for conventional gel electrode and  $29.52 \pm 0.62$  for EFE means that EFE is comparable

to the conventional gel electrode because the average signal quality of EFE is approximately 95% of the signal quality of the conventional gel electrode.

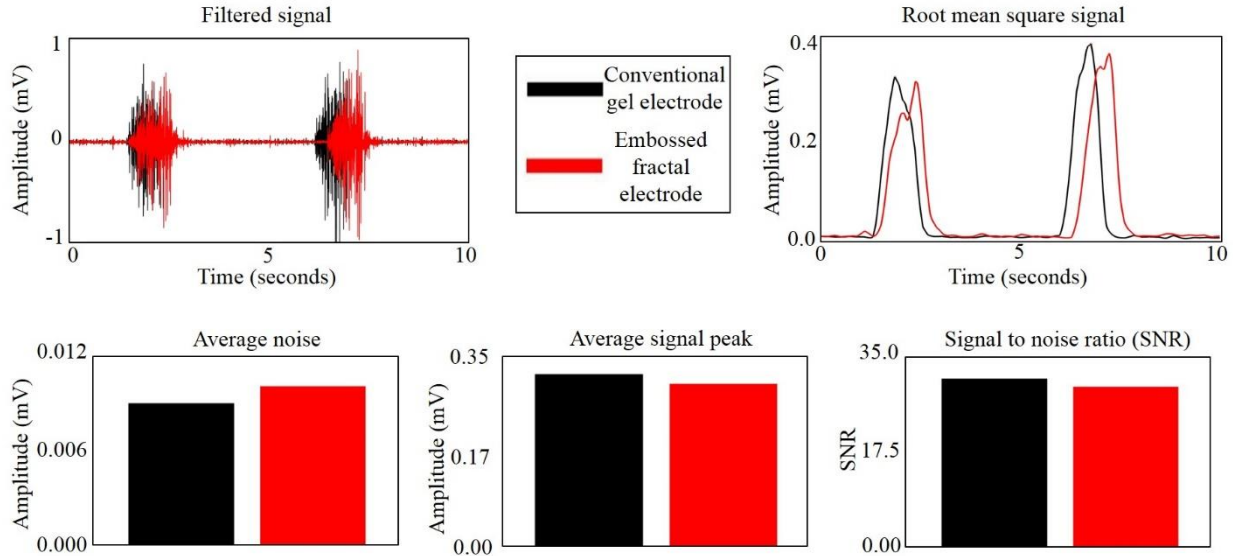


**Figure 17.** EMG signal comparison of conventional gel electrode and embossed fractal electrode.

## 5.2 Electromyogram application to control prosthetic arm.

Since the signal quality of EFE is very close to that of gel electrode, EFE can potentially replace the use of gel electrodes and actual functionality of EFE as electrode for prosthesis needs to be verified. There are different types of prosthesis, for our general purpose of testing basic control of prosthesis, I built my own basic arm model based on the open source information by InMoove. Figure 18 shows the parts of the prosthetic hand, each parts are connected using the bolts through the hole. The movement of each fingers are manipulated by connecting fishing string to each finger using five different rotational motors controlled by Arduino kit.

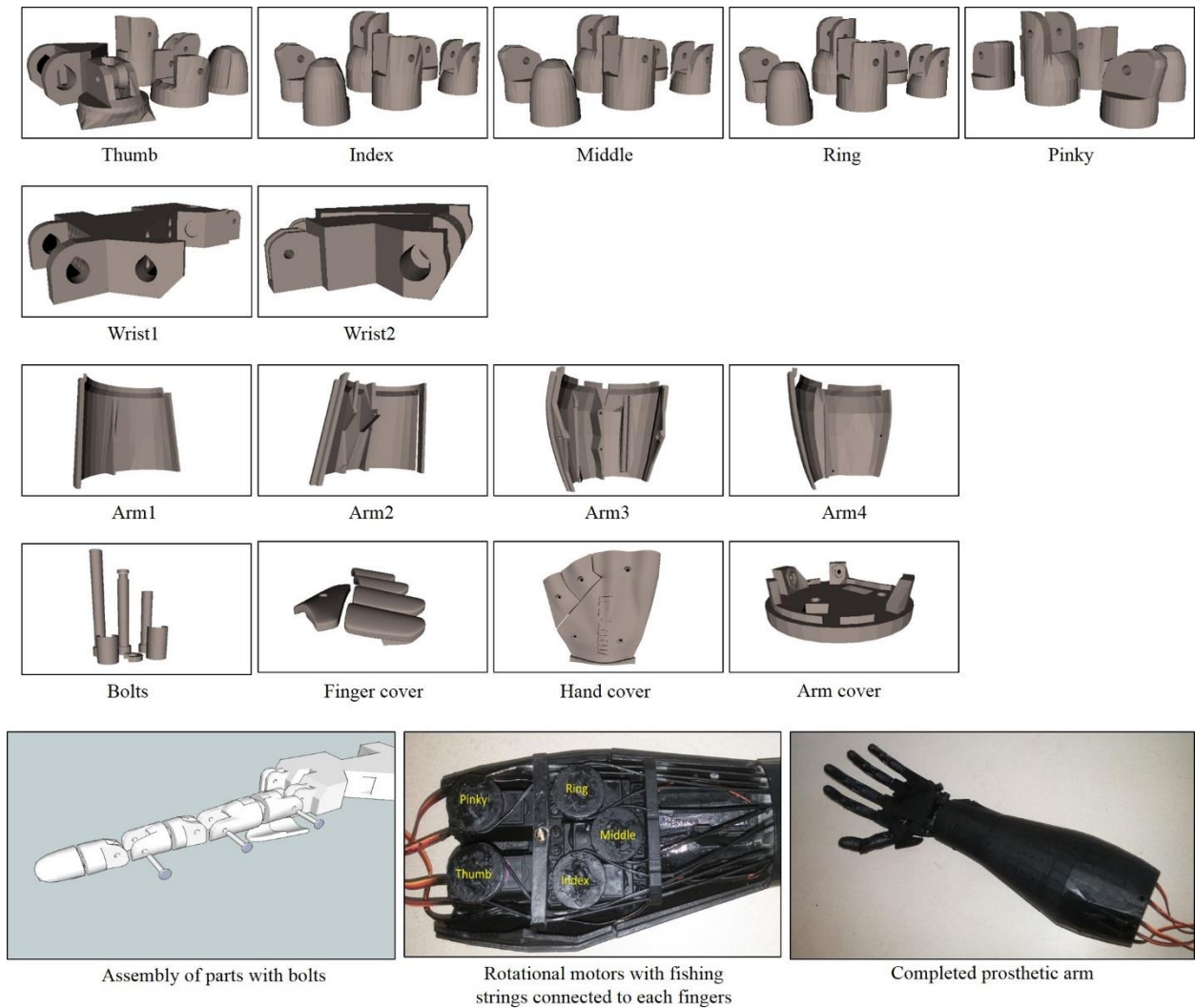


**Figure 18.** Parts of prosthetic arm retrieved from open source InMoove. Image of assembling each parts. Photo of rotational motors assigned for movement of each fingers. Photo of completed prosthetic arm.

For the prosthetic arm control, I classified seven movement, including open, close, thumb, index, middle, ring, and pinky by extracting four features; root mean square, area under the curve, maximum peak, and average of measured EMG signal. Classifications of finger movements require at least three channels on different flexor muscles in the forearm, brachioradialis, palmaris longus, and flexor carpi ulnaris where EMG signals for finger movements can be classified. Figure

19 shows experimental set-up for controlling prosthetic arm with three channels on different muscles in the forearm. Signal from the muscle in three different location are collected by EFE electrodes, then the signal is amplified and transmitted through the data acquisition device to the computer. The signal received by computer is filtered and classified through Matlab and it sends appropriate command to prosthetic arm through Arduino. Details of Matlab code used to collect and classify data are discussed in Appendices IV-XI. The features of the signal measured in each channel are classified into seven different classes. Figure 20 presents different hand motion and classified signal for the different finger motion.

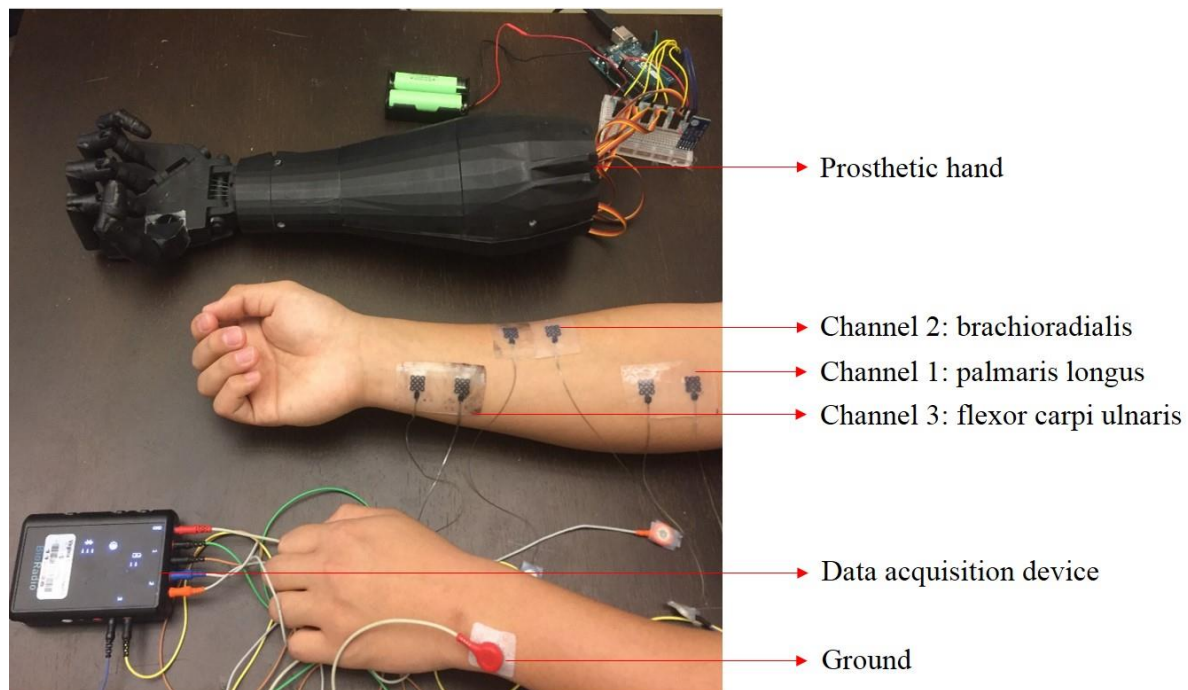


**Figure 19.** Prosthetic arm control set-up with three EFE electrodes on different mounting sites on the forearm.

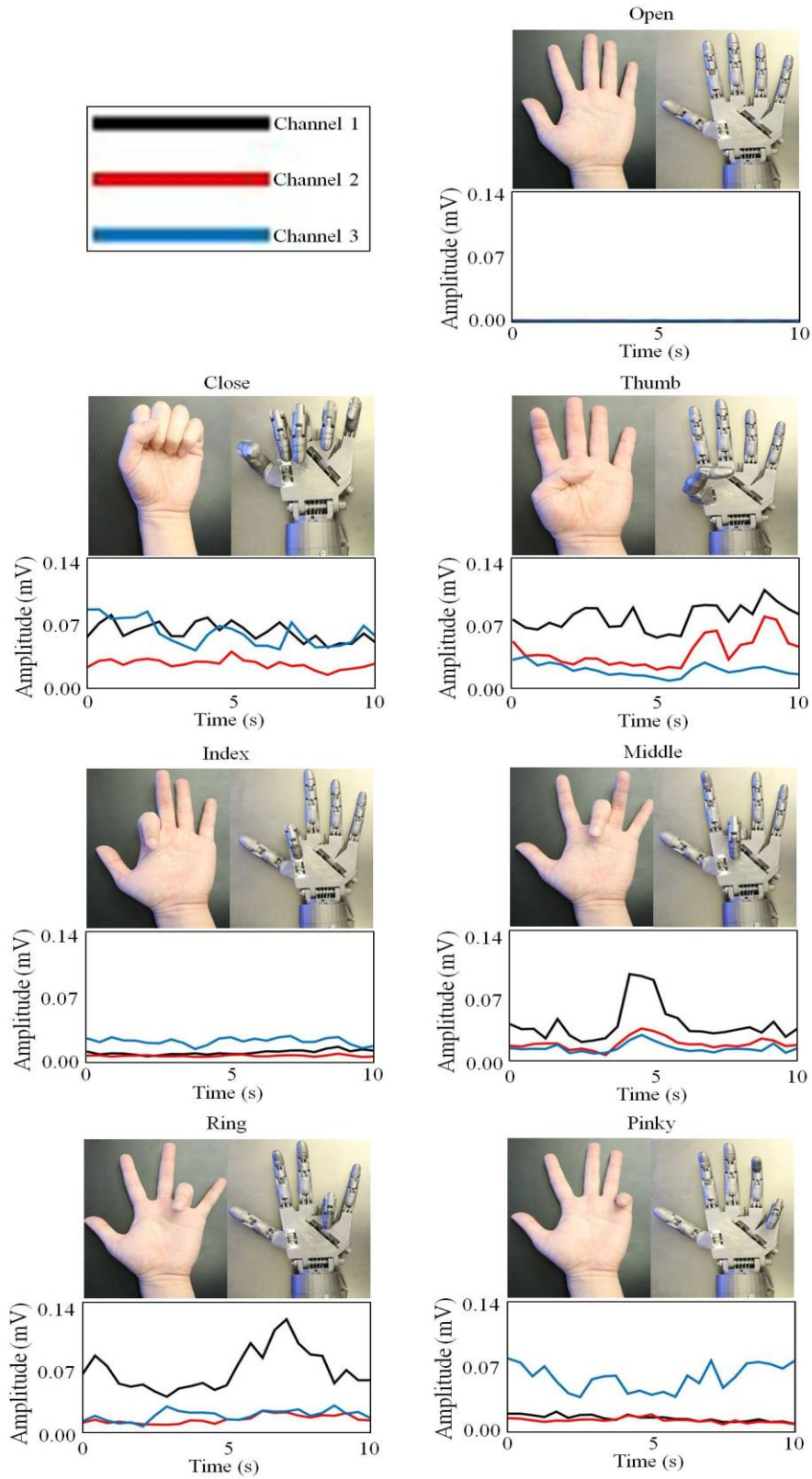


**Figure 20.** Different motions and corresponding signal from each channel.

For hand open motion, signal amplitude is low compare to other movements because muscles do not contract. Reversely, hand close motion has high signal amplitudes in all three channels because folding five fingers requires contraction of all the muscles where electrodes locate. Thumb and ring finger movements show similar signal amplitude at channel one but different amplitude in both channel two and three. Index finger movement is clearly distinguished from other movements because its signal amplitude is lowest among other movements and slightly higher than that of hand open motion. Signal of middle finger movement is similar to that of thumb and ring but it can be classified because signal amplitude of channel one is not as high as when moving thumb and ring fingers. The signal amplitude of moving pinky finger shows highest signal peak at channel three, which means flexor carpi ulnaris contracts the most and other two muscles are not significantly related for pinky finger movement.

Figure 21 presents the accuracy of each gel electrode and EFE for controlling prosthetic arm through confusion matrix that shows cross validation of training data. Details of Matlab code for cross validating data set are discussed in Appendix XII.

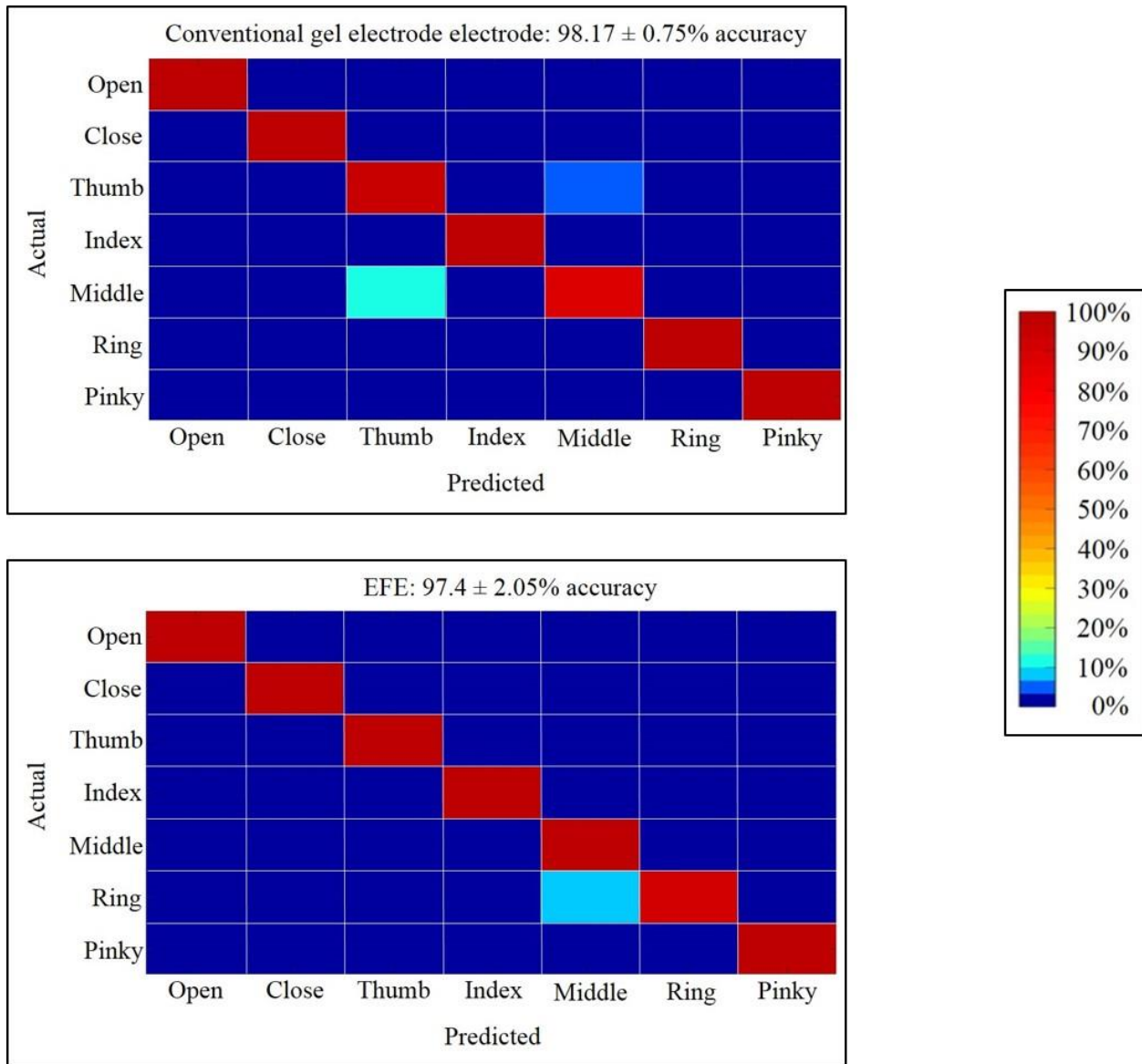


**Figure 21.** Comparison of confusion matrix accuracy (7 classes) between the conventional gel electrode and embossed fractal electrode (EFE).

The accuracy of classifying seven features using the conventional gel electrode is  $98.17 \pm 0.75\%$  and the accuracy of using EFE is  $97.4 \pm 2.05\%$ . Although mean accuracy of EFE is slightly lower than gel electrode, this difference is negligible because the highest accuracy achieved through EFE is 100%. According to the video, the mean accuracy of 97.4% is sufficient to control finger movements of prosthetic arm without any error or misclassification.

## **Chapter 6: Conclusion**

Embossed fractal electrode (EFE) can potentially replace conventional gel electrode and it can overcome some of the weaknesses of conventional gel electrode, which is skin irritation and incapable of utilizing for long-term due to evaporation of the applied gel. Conventional gel electrode has inappropriate adhesion force on the skin, which often cause skin irritation after removal but EFE only has adequate adhesion to make contact on the skin without any irritation. Also, conventional gel electrode often loses its functionality when conductive gel on the surface evaporates over time, however, EFE does not incorporate any conductive gel upon mounting so it is suitable for long-term measurement of any biopotential signal. EFE is stretchable and flexible and fabricated on a thin elastomeric membrane so that it matches with the morphology of the skin, which minimizes gap between electrode and skin that reduces electrode to skin contact impedance. Also, I obtained maximum attainable conductivity of EFE to record good quality signal. Fabricated EFE shows excellent mechanical properties, which allows it to operate on skin without any mechanical failure upon stretching. The prosthetic arm control with EFE was successful and comparable to that of using conventional gel electrode.

Fabrication process of EFE reduces cost and time consuming aspects of other dry electrodes. Previous dry electrodes need expensive machines to fabricate but EFE only requires very basic photolithography process to fabricate its mold. The mold can be reused multiple times until it breaks, which does not occur if handled carefully. From the mold, it only takes few hours to replicate electrode out of the mold.

In the future, study about fabricating EFE in the manufacturing level is required to replace conventional gel electrode with EFE. Also, further study to improve prosthesis is required for more precise movement of the prosthesis for daily use. For example of my prosthetic arm, I can include

precise control of force while folding the finger. Also, more classes for more movement can be added to the interface so that prosthetic arm would include complex movements similar to the performance of real arm.

## List of references

- 1 Xu, B. *et al.* An Epidermal Stimulation and Sensing Platform for Sensorimotor Prosthetic Control, Management of Lower Back Exertion, and Electrical Muscle Activation. *Advanced Materials* **28**, 4462-4471, doi:10.1002/adma.201504155 (2016).
- 2 Kilby, J., Prasad, K. & Mawston, G. Multi-Channel Surface Electromyography Electrodes: A Review. *Sensors* **14****172**, 1 (2016).
- 3 Momen, K., Krishnan, S. & Chau, T. Real-time classification of forearm electromyographic signals corresponding to user-selected intentional movements for multifunction prosthesis control. *IEEE Transactions on Neural Systems and Rehabilitation Engineering* **15**, 535-542 (2007).
- 4 Graupe, D., Magnussen, J. & Beex, A. A microprocessor system for multifunctional control of upper-limb prostheses via myoelectric signal identification. *IEEE Transactions on automatic control* **23**, 538-544 (1978).
- 5 Kiguchi, K., Tanaka, T. & Fukuda, T. Neuro-fuzzy control of a robotic exoskeleton with EMG signals. *IEEE Transactions on fuzzy systems* **12**, 481-490 (2004).
- 6 Quitadamo, L. *et al.* Support vector machines to detect physiological patterns for EEG and EMG-based human-computer interaction: a review. *Journal of Neural Engineering* **14**, 011001 (2017).
- 7 De Luca, C. J., Gilmore, L. D., Kuznetsov, M. & Roy, S. H. Filtering the surface EMG signal: Movement artifact and baseline noise contamination. *Journal of biomechanics* **43**, 1573-1579 (2010).
- 8 Sun, Y. & Yu, X. B. Capacitive biopotential measurement for electrophysiological signal acquisition: A review. *IEEE Sensors Journal* **16**, 2832-2853 (2016).

- 9 Day, S. Important factors in surface EMG measurement. *Bortec Biomedical Ltd publishers*, 1-17 (2002).
- 10 Ferree, T. C., Luu, P., Russell, G. S. & Tucker, D. M. Scalp electrode impedance, infection risk, and EEG data quality. *Clinical Neurophysiology* **112**, 536-544 (2001).
- 11 Chen, Y.-H. *et al.* Soft, comfortable polymer dry electrodes for high quality ECG and EEG recording. *Sensors* **14**, 23758-23780 (2014).
- 12 Löffhede, J., Seoane, F. & Thordstein, M. Textile electrodes for EEG recording—A pilot study. *Sensors* **12**, 16907-16919 (2012).
- 13 Meziane, N., Webster, J., Attari, M. & Nimunkar, A. Dry electrodes for electrocardiography. *Physiological measurement* **34**, R47 (2013).
- 14 Norton, J. J. *et al.* Soft, curved electrode systems capable of integration on the auricle as a persistent brain–computer interface. *Proceedings of the National Academy of Sciences* **112**, 3920-3925 (2015).
- 15 Jung, H.-C. *et al.* CNT/PDMS composite flexible dry electrodes for long-term ECG monitoring. *IEEE Transactions on Biomedical Engineering* **59**, 1472-1479 (2012).
- 16 Kim, T., Park, J., Sohn, J., Cho, D. & Jeon, S. Bioinspired, highly stretchable, and conductive dry adhesives based on 1D–2D hybrid carbon nanocomposites for all-in-one ECG electrodes. *ACS nano* **10**, 4770-4778 (2016).
- 17 Lee, J. H. *et al.* Shear induced CNT/PDMS conducting thin film for electrode cardiogram (ECG) electrode. *BioChip Journal* **6**, 91-98 (2012).
- 18 Reyes, B. A. *et al.* Novel electrodes for underwater ECG monitoring. *IEEE Transactions on Biomedical Engineering* **61**, 1863-1876 (2014).

- 19 Liu, B., Luo, Z., Zhang, W., Tu, Q. & Jin, X. Silver nanowire-composite electrodes for long-term electrocardiogram measurements. *Sensors and Actuators A: Physical* **247**, 459-464 (2016).
- 20 Nitish, V. T. (The Measurement, Instrumentation and Sensors: Handbook, CRC Press LLC, 1999).
- 21 Lee, Y. & Yeo, W.-H. Skin-like electronics for a persistent brain-computer interface. *Journal of Nature and Science* **1**, 132 (2015).
- 22 Plonsey, R. *Bioelectric phenomena*. (Wiley Online Library, 1969).
- 23 Sperelakis, N. *Electrogenesis of Biopotentials in the Cardiovascular System: In the Cardiovascular System*. Vol. 164 (Springer Science & Business Media, 2012).
- 24 Thomas, R. Electrogenic sodium pump in nerve and muscle cells. *Physiological Reviews* **52**, 563-594 (1972).
- 25 Lodish, H. & Zipursky, S. L. Molecular cell biology. *Biochemistry and Molecular Biology Education* **29**, 126-133 (2001).
- 26 Kandel, E. R., Schwartz, J. H. & Jessel, T. M. Essentials of neural science and behavior. (1995).
- 27 Plonsey, R. Bioelectric sources arising in excitable fibers (ALZA lecture). *Annals of biomedical engineering* **16**, 519-546 (1988).
- 28 Reece, J. B. *et al. Campbell biology*. (Pearson Boston, 2011).
- 29 Kiernan, M. C., Lin, C. S., Andersen, K. V., Murray, N. M. & Bostock, H. Clinical evaluation of excitability measures in sensory nerve. *Muscle & nerve* **24**, 883-892 (2001).
- 30 Hodgkin, A. L. The ionic basis of electrical activity in nerve and muscle. *Biological Reviews* **26**, 339-409 (1951).

- 31 Frank, H. Y. & Catterall, W. A. Overview of the voltage-gated sodium channel family. *Genome biology* **4**, 207 (2003).
- 32 Fan, J. A. *et al.* Fractal design concepts for stretchable electronics. *Nature communications* **5** (2014).
- 33 Liao, L.-D., Wang, I.-J., Chen, S.-F., Chang, J.-Y. & Lin, C.-T. Design, fabrication and experimental validation of a novel dry-contact sensor for measuring electroencephalography signals without skin preparation. *Sensors* **11**, 5819-5834 (2011).
- 34 Jeong, J. W. *et al.* Materials and Optimized Designs for Human-Machine Interfaces Via Epidermal Electronics. *Advanced Materials* **25**, 6839-6846 (2013).
- 35 Valdes, L. B. Resistivity measurements on germanium for transistors. *Proceedings of the IRE* **42**, 420-427 (1954).

## **Appendices**

### **I. Mold fabrication method**

1. Clean wafer with acetone, isopropyl alcohol, and deionized water.
2. Spincoat SU-8 2050 at 500rpm for 8seconds and 1300rpm for 30seconds.
3. Soft bake at 65°C for 9minutes.
4. Soft bake at 95°C for 20minutes.
5. Spincoat second SU-8 layer at 500rpm for 8seconds and 1300rpm for 30seconds.
6. Soft bake at 65°C for 9minutes.
7. Soft bake at 95°C for 60minutes.
8. Align pattern and expose UV for 30seconds.
9. Post bake at 65°C for 5minutes.
10. Post bake at 95°C for 15minutes.
11. Develop SU-8 for 25 minutes.
12. Rinse with isopropyl alcohol.

### **II. Replica fabrication method**

1. Silanize the surface of mold.
2. Pour nanocomposite on the mold.
3. Scrape nanocomposite with PDMS block.
4. Place anisotropic conductive film at the contact pad of the replica.
5. Spincoat elastomer at 500rpm for 30seconds.

6. Attach polyvinyl alcohol film on the elastomer.
7. Detach polyvinyl alcohol with the patterned replica.

### III. Matlab code for analyzing EMG signal through SNR

1. `load('');` %load collected signal
2. `data1= loaded file;` %save data into data1
3. `srate = 1000;` %sampling rate
4. `timepoints = [1:length(data1)]/srate;` %convert data into timepoints
5. `frequencies = [0:length(data1)-1]/(length(data1)/srate);` %convert data into frequencies
6. `figure` %raw signal graph 6-9
7. `plot(timepoints,data1(:,1))`
8. `xlabel('Time (seconds)')`
9. `ylabel('amplitude')`
10. `wo = 60/(1000/2); bw = wo/35;` %notch and bandpass filter 11-15
11. `[b,a] = iirnotch(wo,bw);`
12. `High=150*2/sampleRate_BP;`
13. `Low=30/sampleRate_BP;`
14. `[c,d] = butter(6,[Low, High], 'bandpass');`
15. `data2 = filter(c,d,(filter(b,a,data1)));`
16. `figure` %filtered signal graph 16-19
17. `plot(timepoints1,data2)`
18. `xlabel('Time (seconds)')`

```

19. ylabel('Amplitude (V)')
20. data3 = rms(data2, 200, 200-1, 1); %convert into rms and find peaks 20-22
21. data4 = tsmovavg(data3, 's', 200);
22. [pks1, locs1]=findpeaks(data4,'MinPeakHeight',0.00005,'MinPeakWidth',200);
23. figure %graph rms data and find signal to noise ratio 23-29
24. plot(timepoints1,data4,timepoints1(locs1),pks1,'or')
25. sv1=mean(pks1);
26. nv1=mean(data4));
27. snrv1=20*log10(sv1/nv1)
28. xlabel('Time (seconds)')
29. ylabel('Amplitude (V)')

```

#### IV. Matlab code for controlling prosthetic arm.

```

1. current_dir = cd; %Connect Bioradio 1-14
2. [ deviceManager , flag ] = load_API(''); %locate API
3. if ~flag
4. return
5. end
6. [ deviceName , macID , ok ] = BioRadio_Find( deviceManager );
7. if ~ok
8. errordlg('Please select a BioRadio.')
9. return

```

```

10. end
11. [ myDevice, flag ] = BioRadio_Connect ( deviceManager , macID , deviceName );
12. if ~flag
13. return
14. end
15. BioRadioData = BioRadio_StreamTrainer( myDevice , 75, deviceName ); %Real-time
    training
16. Training_RMS = Trainer_RMS(BioRadioData); %Save trained data into classified sets of
    data
17. global blu %Arduino connection 17-19
18. blu=Bluetooth('HC-06',1);
19. fopen(blu);
20. BioRadioData2 = BioRadio_StreamClassifier( myDevice, inf, deviceName, Training_RMS,
    blu); %Real-time control of prosthesis through and saving data sets 20-21
21. myDevice.StopAcquisition; %Disconnecting Bioradio 21-22
22. BioRadio_Disconnect(myDevice);

```

## V. Bioradio\_Connect function

```

1. function [ myDevice, flag ] = BioRadio_Connect ( deviceManager , macID ,
    BioRadioName ) %Bioradio_Connect function

```

```

2. myDevice = []; % Find applicable device name
3. flag = false;
4. try
5. myDevice = deviceManager.GetBluetoothDevice(macID); % instantiate motion sensor object
6. catch
7. errordlg(['Failed to connect to ' BioRadioName '.'])
8. return
9. end
10. flag = true; % successfully connected to all sensors
11. end

```

## VI. Bioradio\_find function

```

1. function [BioRadioName, macID, ok] = BioRadio_Find( deviceManager )
2. dlghandle = helpdlg('Please wait... search in progress.','Searching for Available BioRadios');
3. try
4. BioRadioList = deviceManager.DiscoverBluetoothDevices; %search for BioRadios
5. numavail = BioRadioList.Length;
6. catch
7. numavail = 0;
8. end

```

```

9. close(dlghandle)
10. if numavail<1
11. BioRadioName = [];
12. macID = [];
13. ok = [];
14. return
15. end
16. availableBioRadios = cell(numavail,1);
17. macIDs = cell(numavail,1);
18. for i=1:numavail
19. availableBioRadios1 = char(BioRadioList(i).DeviceId); % pull BioRadio name from list
20. macIDs1 = hex2dec(char(BioRadioList(i).MacId));% pull corresponding mac id from list
21. end
22. [selection, ok] = listdlg('PromptString','Select a BioRadio:',...
23. 'SelectionMode','single','ListString',availableBioRadios); % prompt user to select a BioRadio
24. if ok==0
25. BioRadioName = [];
26. macID = [];
27. ok = [];
28. return
29. else
30. BioRadioName = availableBioRadios{selection};
31. macID = macIDs{selection};

```

32. end

33. end

## VII. Bioradio\_streamtrainer function

```
1. function BioRadioData = BioRadio_StreamTrainer( myDevice , duration ,
    BioRadio_Name )
2. numEnabledBPChannels = double(myDevice.BioPotentialSignals.Count);
3. %If there are no channels enabled on the Bioradio, error:
4. if numEnabledBPChannels == 0
5. myDevice.Disconnect;
6. BioRadioData = [];
7. errordlg('No BioPotential Channels Programmed. Return to BioCapture to Configure.')
8. return
9. end
10. sampleRate_BP = double(myDevice.BioPotentialSignals.SamplesPerSecond); %Setting up
    the real-time window for graph
11. figure
12. axis_handles = zeros(1,numEnabledBPChannels);
13. for ch = 1:numEnabledBPChannels
14. axis_handles(ch) = subplot(length(axis_handles),1,ch);
15. if ch==1
    a. title([char(BioRadio_Name)])
16. end
```

```

17. ylabel([char(myDevice.BioPotentialSignals.Item(ch-1).Name) ' (V)']);
18. hold on
19. end
20. xlabel('Time (s)')
21. linkaxes(axis_handles,'x')
22. BioPotentialSignals = cell(1,numEnabledBPChannels);
23. Filtered = cell(1,numEnabledBPChannels);
24. TrainRMS = cell(1,numEnabledBPChannels);
25. myDevice.StartAcquisition; %Real-time data collection with filters
26. plotWindow = 5;
27. wo = 60/500;
28. bw = wo/35;
29. [b,a] = iirnotch(wo,bw);
30. High=150*2/sampleRate_BP;
31. Low=30/sampleRate_BP;
32. [c,d] = butter(6,[Low, High], 'bandpass');
33. elapsedTime = 0;
34. tic;
35. while elapsedTime < duration
36. pause(0.08)
37. for ch = 1:numEnabledBPChannels
    a. wind = 200;

```

```

b. BioPotentialSignals1 =
    [BioPotentialSignals1;myDevice.BioPotentialSignals.Item(ch-
    1).GetScaledValueArray.double'];

c. Filtered1 = filter(c,d,(filter(b,a,BioPotentialSignals1)));

d. Buff1 = buffer(Filtered1,wind);

e. TrainRMS1 = rms(Buff1)';

f. TrainTRAPZ1 = trapz(Buff1)';

g. TrainMaximum1 = max(Buff1)';

h. TrainAVG1 = mean(Buff1)';

i. if length(Filtered1) <= plotWindow*sampleRate_BP
    i. cla(axis_handles(ch))
    ii. t = (0:(length(Filtered1)-1))*(1/sampleRate_BP);
    iii. plot(axis_handles(ch),t,Filtered1);
    iv. xlim([0 plotWindow])

j. else
    i. if ch==1
    ii. t = ((length(Filtered1)-(plotWindow*sampleRate_BP-
    1)):length(Filtered1))*(1/sampleRate_BP);
    iii. end
    iv. cla(axis_handles(ch))
    v. plot(axis_handles(ch),t,Filtered1(end-plotWindow*sampleRate_BP+1:end));
    vi. xlim([t(end)-plotWindow t(end)])

k. end

```

```

38. end
39. elapsedTime = elapsedTime + toc;
40. tic;
41. end
42. myDevice.StopAcquisition;
43. for ch = 1:numEnabledBPChannels
44. BioPotentialSignals1 = [BioPotentialSignals1;myDevice.BioPotentialSignals.Item(ch-
    1).GetScaledValueArray.double'];
45. t = ((length(Filtered1)-(plotWindow*sampleRate_BP-
    1)):length(Filtered1))*(1/sampleRate_BP);
46. cla(axis_handles(ch))
47. plot(axis_handles(ch),t,Filtered1(end-plotWindow*sampleRate_BP+1:end));
48. xlim([t(end)-plotWindow t(end)])
49. end
50. BioRadioData = cell(1,7); %Saving collected data into different features
51. BioRadioData{1} = BioPotentialSignals;
52. BioRadioData{2} = Filtered;
53. BioRadioData{3} = Buff;
54. BioRadioData{4} = TrainRMS;
55. BioRadioData{5} = TrainAVG;
56. BioRadioData{6} = TrainTRAPZ;
57. BioRadioData{7} = TrainMaximum;
58. end

```

## VIII. Trainer\_RMS function

1. **function** Training\_RMS = Trainer\_RMS(BioRadioData) %Converting gathered data to rms
2. Training1=[BioRadioData{1,4}{1,1}(26:50) BioRadioData{1,4}{1,2}(26:50)  
BioRadioData{1,4}{1,3}(26:50)];
3. Training2=[BioRadioData{1,4}{1,1}(76:100) BioRadioData{1,4}{1,2}(76:100)  
BioRadioData{1,4}{1,3}(76:100)];
4. Training3=[BioRadioData{1,4}{1,1}(126:150) BioRadioData{1,4}{1,2}(126:150)  
BioRadioData{1,4}{1,3}(126:150)];
5. Training4=[BioRadioData{1,4}{1,1}(176:200) BioRadioData{1,4}{1,2}(176:200)  
BioRadioData{1,4}{1,3}(176:200)];
6. Training5=[BioRadioData{1,4}{1,1}(226:250) BioRadioData{1,4}{1,2}(226:250)  
BioRadioData{1,4}{1,3}(226:250)];
7. Training6=[BioRadioData{1,4}{1,1}(276:300) BioRadioData{1,4}{1,2}(276:300)  
BioRadioData{1,4}{1,3}(276:300)];
8. Training7=[BioRadioData{1,4}{1,1}(326:350) BioRadioData{1,4}{1,2}(326:350)  
BioRadioData{1,4}{1,3}(326:350)];
9. Training\_RMS=[Training1;Training2;Training3;Training4;Training5;Training6;Training7];

## IX. Bioradio\_Streamclassifier function

1. **function** BioRadioData2 = BioRadio\_StreamClassifier( myDevice , duration ,  
BioRadio\_Name , Training\_RMS, blu) %Real-time classification

```

2. numEnabledBPChannels = double(myDevice.BioPotentialSignals.Count); %Setting up
   window for real-time graph 2-23
3. if numEnabledBPChannels == 0
4. myDevice.Disconnect;
5. BioRadioData2 = [];
6. errordlg('No BioPotential Channels Programmed. Return to BioCapture to Configure.')
7. return
8. end
9. sampleRate_BP = double(myDevice.BioPotentialSignals.SamplesPerSecond);
10. figure
11. axis_handles = zeros(1,numEnabledBPChannels);
12. for ch = 1:numEnabledBPChannels
13. axis_handles(ch) = subplot(length(axis_handles),1,ch);
14. if ch==1
       a. title([char(BioRadio_Name)])
15. end
16. ylabel([char(myDevice.BioPotentialSignals.Item(ch-1).Name) ' (V)']);
17. hold on
18. end
19. xlabel('Time (s)')
20. linkaxes(axis_handles,'x')
21. BioPotentialSignals = cell(1,numEnabledBPChannels);
22. Filtered = cell(1,numEnabledBPChannels);

```

```
23. TrainRMS = cell(1,numEnabledBPChannels);
24. myDevice.StartAcquisition; %Classification of different motions 24-75
25. plotWindow = 5;
26. group1 = ones(25,1);
27. group2 = ones(25,1)*2;
28. group3 = ones(25,1)*3;
29. group4 = ones(25,1)*4;
30. group5 = ones(25,1)*5;
31. group6 = ones(25,1)*6;
32. group7 = ones(25,1)*7;
33. group = [group1;group2;group3;group4;group5;group6;group7];
34. wo = 60/500;
35. bw = wo/35;
36. [b,a] = iirnotch(wo,bw);
37. High=150*2/sampleRate_BP;
38. Low=30/sampleRate_BP;
39. [c,d] = butter(6,[Low, High], 'bandpass');
40. i = 1;
41. jj = 1;
42. modelength = 5;
43. error_fill_1 = 0;
44. error_fill_2 = 0;
45. error_fill_3 = 0;
```

```

46. error_fill_4 = 0;
47. error_fill_5 = 0;
48. error_fill_6 = 0;
49. error_fill_7 = 0;
50. elapsedTime = 0;
51. tic;
52. while elapsedTime < duration
53. pause(.03)
54. for ch = 1:numEnabledBPChannels
    a. wind = 100;
    b. BioPotentialSignals1 =
        [BioPotentialSignals1;myDevice.BioPotentialSignals.Item(ch-
            1).GetScaledValueArray.double'];
    c. Filtered1 = filter(c,d,(filter(b,a,BioPotentialSignals1)));
    d. Buff1 = buffer(Filtered1,wind);
    e. TrainRMS1 = rms(Buff1)';
    f. TrainAVG1 = mean(Buff1)';
    g. if length(Filtered1) <= plotWindow*sampleRate_BP
        i. cla(axis_handles(ch))
        ii. t = (0:(length(Filtered1)-1))*(1/sampleRate_BP);
        iii. plot(axis_handles(ch),t,Filtered1);
        iv. xlim([0 plotWindow])
    h. else

```

```

        i. if ch==1
        ii. t = ((length(Filtered1)-(plotWindow*sampleRate_BP-
                1)):length(Filtered1))*(1/sampleRate_BP);
        iii. end
        iv. cla(axis_handles(ch))
        v. plot(axis_handles(ch),t,Filtered1(end-plotWindow*sampleRate_BP+1:end));
        vi. xlim([t(end)-plotWindow t(end)])
    i. end
55. end
56. if length(TrainRMS{1})>=5
        a. kick = TrainRMS{1}(length(TrainRMS{1}));
57. else kick = 0;
58. end
59. if length(TrainRMS{2})>=5
        a. punch = TrainRMS{2}(length(TrainRMS{2}));
60. else punch = 0;
61. end
62. if length(TrainRMS{3})>=5
        a. karatechop = TrainRMS{3}(length(TrainRMS{3}));
63. else karatechop = 0;
64. end
65. if length(TrainRMS1)>5
66. sample = [kick punch karatechop];

```

```

67. clss(i) = classify(sample,Training_RMS,group);
68. if i > modelength
    a. classmode(jj) = mode(clss(i-modelength:i));
    b. if classmode(jj) == 1
        i. error_fill_1 = error_fill_1 + 1;
        ii. error_fill_2 = 0;
        iii. error_fill_3 = 0;
        iv. error_fill_4 = 0;
        v. error_fill_5 = 0;
        vi. error_fill_6 = 0;
        vii. error_fill_7 = 0;
        viii. if error_fill_1 >= 8;
            ix. disp('hand open')
            x. fwrite(blu,1)
            xi. error_fill_1 = 0;
            xii. end
        xiii. elseif classmode(jj) == 2
            xiv. error_fill_2 = error_fill_2 + 1;
            xv. error_fill_1 = 0;
            xvi. error_fill_3 = 0;
            xvii. error_fill_4 = 0;
            xviii. error_fill_5 = 0;

```

- xix. `error_fill_6 = 0;`
  - xx. `error_fill_7 = 0;`
  - xxi. `if error_fill_2 >= 8;`
  - xxii. `disp('hand closed')`
  - xxiii. `fwrite(blu,2);`
  - xxiv. `error_fill_2 = 0;`
  - xxv. `end`
- c. `elseif classmode(jj) == 3`
- i. `error_fill_3 = error_fill_3 + 1;`
  - ii. `error_fill_1 = 0;`
  - iii. `error_fill_2 = 0;`
  - iv. `error_fill_4 = 0;`
  - v. `error_fill_5 = 0;`
  - vi. `error_fill_6 = 0;`
  - vii. `error_fill_7 = 0;`
  - viii. `if error_fill_3 >= 8;`
  - ix. `disp('thumb closed')`
  - x. `fwrite(blu,3);`
  - xi. `error_fill_3 = 0;`
  - xii. `end`
- d. `elseif classmode(jj) == 4`
- i. `error_fill_4 = error_fill_4 + 1;`
  - ii. `error_fill_1 = 0;`

```
iii. error_fill_2 = 0;
iv. error_fill_3 = 0;
v. error_fill_5 = 0;
vi. error_fill_6 = 0;
vii. error_fill_7 = 0;
viii. if error_fill_4 >= 8;
ix. disp('index closed')
x. fwrite(blu,4);
xi. error_fill_4 = 0;

xii. end

xiii. elseif classmode(jj) == 5
xiv. error_fill_5 = error_fill_5 + 1;
xv. error_fill_1 = 0;
xvi. error_fill_2 = 0;
xvii. error_fill_3 = 0;
xviii. error_fill_4 = 0;
xix. error_fill_6 = 0;
xx. error_fill_7 = 0;
xxi. if error_fill_5 >= 8;
xxii. disp('middle closed')
xxiii. fwrite(blu,5);
xxiv. error_fill_5 = 0;
```

xxv. `end`

- e. `elseif classmode(jj) == 6`
  - i. `error_fill_6 = error_fill_6 + 1;`
  - ii. `error_fill_1 = 0;`
  - iii. `error_fill_2 = 0;`
  - iv. `error_fill_3 = 0;`
  - v. `error_fill_4 = 0;`
  - vi. `error_fill_5 = 0;`
  - vii. `error_fill_7 = 0;`
- f. `if error_fill_6 >= 8;`
  - i. `disp('ring closed')`
  - ii. `fwrite(blu,6)`
  - iii. `error_fill_6 = 0;`
- g. `end`
  - i. `elseif classmode(jj) == 7`
  - ii. `error_fill_7 = error_fill_7 + 1;`
  - iii. `error_fill_1 = 0;`
  - iv. `error_fill_2 = 0;`
  - v. `error_fill_3 = 0;`
  - vi. `error_fill_4 = 0;`
  - vii. `error_fill_5 = 0;`
  - viii. `error_fill_6 = 0;`
- h. `if error_fill_7 >= 8;`

```

        i. disp('pinky closed')
        ii. fwrite(blu,7)
        iii. error_fill_7 = 0;
    i. end
    j. end
69. end
70. jj=jj+1;
71. end
72. i = i+1;
73. elapsedTime = elapsedTime + toc;
74. tic;
75. end
76. myDevice.StopAcquisition; %Stop data acquisition
77. for ch = 1:numEnabledBPChannels
78. BioPotentialSignals1 = [BioPotentialSignals1;myDevice.BioPotentialSignals.Item(ch-
    1).GetScaledValueArray.double'];
79. t = ((length(Filtered1)-(plotWindow*sampleRate_BP-
    1)):length(Filtered1))*(1/sampleRate_BP);
80. cla(axis_handles(ch))
81. plot(axis_handles(ch),t,Filtered1(end-plotWindow*sampleRate_BP+1:end));
82. xlim([t(end)-plotWindow t(end)])
83. end
84. BioRadioData2 = cell(1,4);

```

85. BioRadioData2{1} = BioPotentialSignals;
86. BioRadioData2{2} = Filtered;
87. BioRadioData2{3} = Buff;
88. BioRadioData2{4} = TrainRMS;
89. BioRadioData2{5} = TrainAVG;
90. end

## X. Trainer\_AVG function

1. **function** Training\_AVG = Trainer\_AVG(BioRadioData) %Collecting average of data sets
2. Training1=[BioRadioData{1,5}{1,1}(26:50) BioRadioData{1,5}{1,2}(26:50)  
BioRadioData{1,5}{1,3}(26:50)];
3. Training2=[BioRadioData{1,5}{1,1}(76:100) BioRadioData{1,5}{1,2}(76:100)  
BioRadioData{1,5}{1,3}(76:100)];
4. Training3=[BioRadioData{1,5}{1,1}(126:150) BioRadioData{1,5}{1,2}(126:150)  
BioRadioData{1,5}{1,3}(126:150)];
5. Training4=[BioRadioData{1,5}{1,1}(176:200) BioRadioData{1,5}{1,2}(176:200)  
BioRadioData{1,5}{1,3}(176:200)];
6. Training5=[BioRadioData{1,5}{1,1}(226:250) BioRadioData{1,5}{1,2}(226:250)  
BioRadioData{1,5}{1,3}(226:250)];
7. Training6=[BioRadioData{1,5}{1,1}(276:300) BioRadioData{1,5}{1,2}(276:300)  
BioRadioData{1,5}{1,3}(276:300)];

8. Training7=[BioRadioData{1,5}{1,1}(326:350) BioRadioData{1,5}{1,2}(326:350) BioRadioData{1,5}{1,3}(326:350)];
9. Training\_AVG=[Training1;Training2;Training3;Training4;Training5;Training6;Training7];

## **XI. Bioradio\_Disconnect function**

1. `function` BioRadio\_Disconnect ( myDevice )
2. myDevice.Disconnect;

## **XII. Cross-validation confusion matrix**

1. `load('')` %Load collected data sets
2. TrainFeature1 =  
[BioRadioData{1,4}{1,1},BioRadioData{1,4}{1,2},BioRadioData{1,4}{1,3}]; %Extract training data set that will be classified
3. `for` ch = 1:3
4. TrainFeature(:,ch) =  
[BioRadioData{1,4}{1,ch}(26:50);BioRadioData{1,4}{1,ch}(76:100);BioRadioData{1,4}{1,ch}(126:150);BioRadioData{1,4}{1,ch}(176:200);...  
BioRadioData{1,4}{1,ch}(226:250);BioRadioData{1,4}{1,ch}(276:300);BioRadioData{1,4}{1,ch}(326:350)];
5. `end`
7. TrainFeature=Training\_RMS
8. CLASS(1:25) = 1; %Assign classes

```

9. CLASS(26:50) = 2;
10. CLASS(51:75) = 3;
11. CLASS(76:100) = 4;
12. CLASS(101:125) = 5;
13. CLASS(126:150) = 6;
14. CLASS(151:175) = 7;
15. template = templateSVM(...
16. 'KernelFunction', 'polynomial', ...
17. 'PolynomialOrder', 2, ...
18. 'KernelScale', 'auto', ...
19. 'BoxConstraint', 1, ...
20. 'Standardize', true);
21. classificationSVM = fitcecoc(...
22. TrainFeature, ...
23. CLASS, ...
24. 'Learners', template, ...
25. 'Coding', 'onevsone', ...
26. 'ClassNames', [1; 2; 3; 4; 5; 6; 7]);
27. partitionedModel = crossval(classificationSVM, 'KFold', 5); %Assign cross validation with
    SVM 5 fold
28. % Compute validation accuracy
29. validationAccuracy = 1 - kfoldLoss(partitionedModel, 'LossFun', 'ClassifError')
30. Accuracy(1) = validationAccuracy;

```

```

31. % Compute validation predictions and scores
32. [validationPredictions, validationScores] = kfoldPredict(partitionedModel);
33. C = confusionmat(CLASS,validationPredictions)
34. cMatLDA2(1,:,:) = C;
35. ClassificationLearner =
    table([TrainFeature(:,1),TrainFeature(:,2),TrainFeature(:,3)],CLASS');
36. labels={'1','2','3','4','5','6','7'}; %Confusion matrix design
37. ActualTotalNumber = sum(squeeze(sum(cMatLDA2,1)),2);
38. SqueezedcMatLDA2 = squeeze(sum(cMatLDA2,1));
39. for z = 1:7
40. cMatLDAPercent(z,:) = (SqueezedcMatLDA2(z,:)./(ActualTotalNumber(z)))*100;
41. end
42. heatmap(cMatLDAPercent, labels, labels,
    '%0.2f%%','Colormap','jet','ShowAllTicks',0,'UseLogColorMap',true,'Colorbar',true,'ColorLe
    vels',30,'MaxColorValue',100,'MinColorValue',0);
43. xlabel('Predicted'),ylabel('Actual'),title('Confusion Matrix for One Eye')
44. xtickangle(60)

```

## Vita

Dong Sup Lee was born on April 23, 1988, in Seoul, South Korea, and is a Korean citizen. He graduated from International School of Manila, Fort Bonifacio, Philippines in 2007. He served in Korean military from October 2009 to June 2011. He received his Bachelor of Science in Chemistry from University of Illinois at Urbana-Champaign, Champaign, Illinois in 2013, and worked as research assistant in Rogers Group in Champaign for 6 months.

### List of publications (*co-author*)

1. "Multifunctional Skin-like Electronics for Quantitative, Clinical Monitoring of Cutaneous Wound Healing", *Nature Communications*, 2013
  - *I was acknowledged in this work based on my contribution: material preparation and data analysis.*
2. "Fractal Design Concepts for Stretchable Electronics", *Nature Communication*, 2014
  - *I was acknowledged in this work based on my contribution: material preparation and data analysis.*
3. "Soft, curved electrode systems capable of integration on the auricle as a persistent brain-computer interface", *Proceedings of the National Academy of Sciences of the United States of America (PNAS)*, 2015
4. "Fabrication and Characterization of a Conformal Skin-Like Electronic System for Quantitative, Cutaneous Wound Management", *Journal of visualized Experiments*, 2015
5. "Soft, Conformal Bioelectronics for a Wireless Human-Wheelchair Interface",

*Biosensors and Bioelectronics*, 2017

6. “Soft Electronics Enabled Ergonomic Human-Computer Interaction for Swallowing Training in Dysphagia Rehabilitation”, *Scientific Reports (Nature Group)*, 2017

### **List of Teaching experiences/Awards**

1. Volunteer work for helping the physically impaired people, 2009
2. Mentor(Teaching)- Volunteer teaching math/english for middle/high school students from low-wage income families, Summer 2009
3. Best student presentation award in Virginia Academy of Science annual meeting, 2015
4. Teaching assistant- Nuclear Power Plants, Summer 2015
5. Mentor(advisor)- Dean’s Early Research Initiative  
-Microneedle patch project, Fall 2015- April 2016
6. Mentor(advisor)- Vertically Integrated Projects: SKINTRONICS  
-Microneedle patch project, Spring 2016  
-Carbon based electrophysiological signal sensor, Fall 2016